



## Research paper

## Solvothermal modification of magnesium phthalocyanine

Jan Janczak

Institute of Low Temperature and Structure Research, Polish Academy of Sciences, P.O. Box 1410, 50-950 Wrocław, Poland

## ARTICLE INFO

## Article history:

Received 15 November 2017

Received in revised form 2 February 2018

Accepted 9 March 2018

Available online 4 April 2018

## Keywords:

Magnesium phthalocyanine derivatives

Crystal structure

Reactivity

UV–Vis spectroscopy

Molecular electrostatic potential

TD-DFT

## ABSTRACT

Reactivity of magnesium phthalocyanine (MgPc) in the dry 3,4-lutidine (3,4-lut), in the 3,4-lut/DMSO, in DMSO and in 3,4-lut/acetylacetone (acacH) systems has been investigated. Reaction of MgPc with dry 3,4-lut leads to formation of MgPc(3,4-lut) compound (**1**), in which the Mg atom is characterised by rarely encountering in magnesium phthalocyanines 4 + 1 N-type of coordination. In presence of the water tracer, depending on the reaction conditions and the 3,4-lut quantity in the MgPc/3,4-lut/DMSO system the solvothermal reaction leads to formation of three complexes in the crystalline form: MgPc(H<sub>2</sub>O)<sub>2</sub>(3,4-lut) – (**2**), [MgPc(3,4-lut)][MgPc(H<sub>2</sub>O)<sub>2</sub>(3,4-lut)]·½(3,4-lut) – (**3**) and [MgPc(H<sub>2</sub>O)<sub>2</sub>(3,4-lut)][MgPc(DMSO)]·½(DMSO) – (**4**). Reaction of MgPc with DMSO yields crystalline MgPc(DMSO) complex (**5**). In these complexes in the solid-state the central Mg atom of MgPc exhibits 4 + 1 coordination. The reaction of MgPc in the case of 3,4-lut/acacH system leads to demetallation of MgPc and formation of crystalline Mg(acac)<sub>2</sub>(H<sub>2</sub>O)<sub>2</sub> compound (**6**) that after several days at ambient air in the mother liquor transforms into organic crystalline compound of C<sub>10</sub>H<sub>12</sub>O<sub>2</sub> (**7**). The structure of **1–7** has been determined by X-ray single crystal diffraction. All MgPc-derivatives (**1–5**) were characterised by thermogravimetric analysis. Partial MO energy diagrams and the calculated absorption spectra of the MgPc-derivatives were compared with the experimental electronic absorption spectra in 3,4-lutidine and DMSO solutions. These results point that the axial ligation of MgPc by O- and N-donor ligands do not change significantly the energy gap of the HOMO–LUMO levels which is compared with that of the parent MgPc pigment.

© 2018 Elsevier B.V. All rights reserved.

## 1. Introduction

Ever since Linstead's report in 1934 [1] phthalocyanine and its metal complexes are used as industrial dyes and pigments. Nevertheless, novel application of these macrocycles, which structurally consist of four isoindole units connected by azamethine bridges to form an 18- $\pi$  electron aromatic macrocycles, are extensively studied. They are intensively studied as multiply functional materials useful for modern technology [2–5]. They can be useful as organic materials for electronic, optoelectronic and photoelectronic devices like as recordable disks (CD), active matrix liquid crystals displays, photoconductors in laser printers and solar cells [6–10]. Moreover, metallophthalocyanines have been applied as photosensitizers for photodynamic therapy, both in their free form as well as after incorporation into liposomes [11–17]. PDT is a cancer treatment that necessitates the activation of a photosensitizer in the cancer cell with the appropriate wave-length of light [12].

Our interest in magnesium phthalocyanine and its 4 + 1 and 4 + 2 coordinated derivatives (MgPcL and MgPcL<sub>2</sub>, where L is

N- or O-donating ligands) arises from their similarity and relationships to the chlorophyll that provides the possibility to them to be used as synthetic model [18]. MgPc, similar to other metal(II) phthalocyanines, crystallises in two polymorphic forms  $\alpha$  and  $\beta$ . However, the X-ray single crystal structure has been determined only for its  $\beta$  modification [19]. Additionally, it has been stated that the crystals of MgPc are unstable in ambient atmosphere forming complexes with the compositions of (MgPc)<sub>2</sub>-O<sub>2</sub> and (MgPc)<sub>2</sub>N<sub>2</sub> [20]. The formation of the oxygenated magnesium phthalocyanine complex has been confirmed by the X-ray single crystal analysis [21]. In the solid state MgPc exhibits an intense absorption band in the near-IR spectral region due to its non-planar nature that arises from the interaction of electropositively polarised Mg center of one molecule with the electronegatively polarised N-azamethine atom of a neighbouring MgPc molecule along the stacking arrangement [19,22].

A wide application of metallophthalocyanines including the MgPc for technological purposes is limited by their relatively low solubility in most organic solvents. The well-known way to tune the application properties of metal(II) phthalocyanine complexes is modify the phthalocyaninato(2–) macroring by the aryl,

E-mail address: [j.janczak@int.pan.wroc.pl](mailto:j.janczak@int.pan.wroc.pl)

alkyl and other substituents [23–29] or by additive metal center complexation [30–33]. Some of axially ligated magnesium phthalocyanine derivatives MgPc(L) with different ligands like as F, Cl, Br and triphenylphosphine oxide crystallise as solvate and their molecular structures were determined by the Homborg group [34,35]. The role of the peripheral substituents in the chemistry of phthalocyanines and their optical properties was the subject of some reviews [36–38]. Both methods improve the solubility of the M(II)Pc-complexes due to the steric hindrance of axial ligands or substituents of hydrogen atoms on phthalocyaninate(2–) macrocycle that lowers the  $\pi$ - $\pi$  interactions as well as the aggregation in solutions [39–41]. Correspondingly it has been well experienced that the feature of MPC's may be tuned by their annealing in various solvents. The MPC's in such processes undergo not only the recrystallization or purification, but they may interact with the solvent molecules forming MPC-derivatives [42–47]. The interaction of some MPC's with solvent molecules resulting in their decomposition was found in the indium monophthalocyanine [48]. Another examples of the active role of the solvents are interactions of the hafnium monophthalocyanine and hafnium diphthalocyanine complexes with acetylacetone, benzonitrile and 4-methylpyridine yielding to formation of novel hafnium phthalocyaninate complexes [49], as well as the formation of the holmium open phthalocyanine (oPc) complex that has been isolated during investigation of the reactivity of iodine doped holmium diphthalocyanine (HoPc<sub>2</sub>I) in the acetylacetone-water system [50]. The active role of MgPc in the catalytic transformation of the cyano group in the organic cyano compounds has been confirmed [51].

Quite recently, solvothermal reaction of MgPc in dry 3,5-lutidine, in 3,5-lutidine/DMSO and in 3,5-lutidine/acetylacetone systems resulting in the formation of new complexes in the crystalline form has been performed [52]. In the present work, the investigation of the interaction of the MgPc with the solvent molecules, i.e. in dry 3,4-lutidine, in 3,4-lutidine/DMSO, in DMSO and in 3,4-lutidine/acetylacetone systems, is the aim of this work. The solvothermal reaction of the MgPc in such systems lead to formation of the new products in the crystalline form. Additionally, other behaviour of the 3,4-lutidine in relation to 3,5-lutidine in these systems will be discussed.

## 2. Experimental

### 2.1. Materials and methods

Crystalline form of MgPc was obtained as described previously [19]. 3,4-lutidine, DMSO and acetylacetone were obtained from Aldrich. The composition of the obtained crystals was checked with a Perkin-Elmer 2400 elemental analyser and with energy dispersive spectroscopy (EDS). EDS spectra were acquired and analysed using an EDAX Pegasus XM4 spectrometer with SDD Apollo 4D detector mounted on a FEI Nova NanoSEM 230 microscope. In addition the elemental analysis was carried out also with a Perkin-Elmer 240 elemental analyzer. Measurements of the UV-Vis spectra were carried out at room temperature using a Cary-Varian 2300 spectrometer. The UV-Vis spectra were recorded in 3,4-lutidine or DMSO solution ( $c = 10^{-6}$  mol/l). Thermal analysis was carried out on a Linseis L81 thermobalance apparatus with Pt crucibles. The initial sample mass was about 25 mg. Powder Al<sub>2</sub>O<sub>3</sub> was used as a reference. The measurements were performed under static air on heating from room temperature to 300 °C at the heating rate of 5 °C min<sup>-1</sup>. The rest of the samples after TG analyses were checked on a PANanalytical X'Pert diffractometer equipped with a Cu-K $\alpha$  radiation source ( $\lambda = 1.54182$  Å) at room temperature.

### 2.2. Preparation procedure

#### 2.2.1. Synthesis of MgPc(3,4-lut) complex (1)

Freshly obtained crystalline MgPc (0.15 g) was added to the dry 3,4-lut (10 mL). The suspension of MgPc in 3,4-lut was degassed and sealed under reduced pressure in a glass ampoule. Next the ampoule was heated at 160 °C for two days and then it was cooled to the room temperature. After such processing several well-developed single crystals of **1** were obtained. The crystals of **1** were separated by filtration and dried in air. Yield: 0.152 g (85%). Analysis: found: Mg, 3.81; C, 72.67; N, 19.64 and H, 3.88%. Calculated for C<sub>39</sub>H<sub>25</sub>N<sub>9</sub>Mg: Mg, 3.77; C, 72.74; N, 19.58 and H, 3.91%.

#### 2.2.2. Synthesis of MgPc(H<sub>2</sub>O)·2(3,4-lut) complex (2)

MgPc (0.2 g) was added to a mixture of 3,4-lut (10 mL) with DMSO (1 mL). The MgPc in the 3,4-lut/DMSO (10:1) system was degassed and sealed under reduced pressure in a glass ampoule, and it was thermally processed at 130 °C during two days and then it was cooled to the room temperature. After such processing blue-violet well-developed single crystals of **2** were obtained. The crystals of **2** were separated by filtration washed with diethyl ether and dried in air. Yield: 0.235 g (82%). Analysis: found: Mg, 3.15; C, 71.72; N, 18.15; O, 2.18 and H, 4.80%. Calculated for C<sub>46</sub>H<sub>36</sub>N<sub>10</sub>OMg: Mg, 3.16; C, 71.83; N, 18.11; O, 2.28 and H, 4.62%.

#### 2.2.3. Synthesis of [MgPc(3,4-lut)] [MgPc(H<sub>2</sub>O)·2(3,4-lut)]·½(3,4-lut) – (3)

MgPc (0.2 g) was added to a mixture of 3,4-lut (10 mL) with DMSO (2 mL). The suspension of MgPc in 3,4-lut/DMSO (5:1) was degassed and sealed under reduced pressure in a glass ampoule. Solvothermal processing was identical as used for the crystals **2**. The obtained crystals **3** were separated by filtration and dried in air. Yield: 0.152 g (56%). Analysis: found: Mg, 3.39; C, 72.04; N, 18.55; O, 1.18 and H, 4.48%. Calculated for C<sub>88.5</sub>H<sub>65.5</sub>N<sub>19.5</sub>OMg<sub>2</sub>: Mg, 2.62; C, 72.98; N, 17.32; O, 1.72 and H, 5.36%.

#### 2.2.4. Synthesis of [MgPc(H<sub>2</sub>O)·(3,4-lut)] [MgPc(DMSO)]·½(DMSO) – (4)

MgPc (0.2 g) was added to a mixture of 3,4-lut (8 mL) with DMSO (8 mL). The suspension of MgPc in 3,4-lut/DMSO was degassed and sealed under reduced pressure in a glass ampoule. The ampoule with the suspension was thermally processed at 130 °C during two days and then it was cooled to the room temperature. After such processing blue-violet well-developed single crystals of **4** were obtained. The crystals of **4** were separated by filtration washed with diethyl ether and dried in air. Yield: 0.192 g (78%). Analysis: found: Mg, 3.65; C, 67.58; N, 18.16; O, 3.11, S, 3.58 and H, 3.92%. Calculated for C<sub>74</sub>H<sub>52</sub>N<sub>17</sub>O<sub>2.5</sub>S<sub>1.5</sub>Mg<sub>2</sub>: Mg, 3.69; C, 67.44; N, 18.09; O, 3.14, S, 3.66 and H, 3.98%.

#### 2.2.5. Synthesis of MgPc(DMSO) complex – (5)

Freshly obtained crystalline MgPc (0.15 g) was added to the DMSO (15 mL). The suspension of MgPc in DMSO was degassed and sealed under reduced pressure in a glass ampoule. Next the ampoule was heated at 170 °C for one day and then it was cooled to the room temperature. After such processing several well-developed blue-violet single crystals of **5** were obtained. The crystals of **5** were separated by filtration. The crystals of **5** were separated by filtration washed with diethyl ether and dried in air. Yield: 0.155 g (90%). Analysis: found: Mg, 3.98; C, 66.54; N, 18.12; O, 2.72; S, 5.11 and H, 3.53%. Calculated for C<sub>32</sub>H<sub>22</sub>N<sub>8</sub>OSMg: Mg, 3.95; C, 66.41; N, 18.22, O, 2.60; S, 5.21 and H, 3.61%.

#### 2.2.6. Synthesis of Mg(acac)<sub>2</sub>(H<sub>2</sub>O)<sub>2</sub> – (6) and C<sub>10</sub>H<sub>12</sub>O<sub>2</sub> – (7)

MgPc (0.15 g) was added to a mixture of 3,4-lut (6 mL) with acacH (6.0 mL). The MgPc in the 3,4-lut/acacH system was

degassed and sealed under reduced pressure in a glass ampoule. It was thermally processed at 120 °C during two days and then it was cooled to the room temperature. Next the ampoule was opened and left for several days for crystallization. After two-three weeks colourless well-developed rectangular single crystals of **6** were obtained. Several crystals of **6** were separated from the solution for the X-ray single crystal and elemental analysis. Found: Mg, 9.35; C, 46.33; O, 37.22 and H, 7.10%. Calculated for  $C_{10}H_{18}O_6Mg$ : Mg, 0.40; C, 46.45; O, 37.13 and H, 7.02%. The rest of solution along with colourless crystal **6** was left through a few next days and after two weeks crystal **6** disappeared (underwent dissolving in solution) and after three consecutive weeks new colourless crystals suitable for the X-ray analysis with the needle shape appeared in solution (**7**). The crystals **7** were separated by filtration and dried in air. Analysis: found: C, 73.22; O, 19.57 and H, 7.21%. Calculated for  $C_{10}H_{12}O_2$ : C, 73.15; O, 19.49 and H, 7.36%.

### 2.3. X-ray crystallography

The obtained single crystals of **1–7** were used for data collection on a four-circle KUMA KM4 diffractometer equipped with two-dimensional CCD area detector. The graphite monochromatized Mo-K $\alpha$  radiation ( $\lambda = 0.71073 \text{ \AA}$ ) and the  $\omega$ -scan technique ( $\Delta\omega = 1^\circ$ ) were used for data collection. Lattice parameters were refined by the least-squares methods on all reflections positions. One image was monitored as a standard after every 40 images for a control of stability of the crystal. Data collection and reduction along with absorption correction were performed using CrysAlis software package [53]. The structures were solved by direct methods using *SHELXS-97* [54] giving positions of almost all non-hydrogen atoms. Initially, the structures were refined using *SHELXL-2014* [55] with the anisotropic thermal displacement parameters. Hydrogen atoms of the phthalocyanine moiety were located on

difference Fourier maps, but in the final refinement positions of all hydrogen atoms were constrained: thermal parameters and distances. Visualizations of the structures were made with the Diamond 3.0 program [56]. Details of the data collection parameters, crystallographic data and final agreement parameters are collected in Table 1.

### 2.4. Theoretical calculations

Molecular orbital calculations with full geometry optimization of ligated MgPc by 3,4-lutidine, MgPc(3,4-lut) and aquamagnesium phthalocyanine MgPc(H<sub>2</sub>O) and the Mg(DMSO) were performed with the Gaussian09 program package [57]. All calculations were carried out with the DFT method using the Becke3-Lee-Yang-Parr correlation functional (B3LYP) [58–60] with the 6–31+G\* basis set assuming the geometry resulting from the X-ray diffraction study as the starting structure. The calculations were also performed for the substrates MgPc, 3,4-lut, DMSO and acacH molecules. As convergence criterions the threshold limits of 0.00025 and 0.0012 a.u. were applied for the maximum force and the displacement, respectively. The three-dimensional molecular electrostatic potential (3D MESP) maps are obtained on the basis of the DFT (B3LYP/6–31+G(d)) optimised geometries of reacted molecules as well as for the reaction product molecules. The calculated 3D MESP is mapped onto the total electron density isosurface ( $0.008 \text{ e\AA}^{-3}$ ) for each molecule. The colour code of MESP maps is in the range of  $-0.05$  (red) to  $0.05 \text{ e\AA}^{-1}$  (blue). After the geometry optimization, the time-dependent (TD) DFT calculations [61,62] were performed to evaluate the absorption spectrum employing the same level and basis sets. All stationary points were optimised without any symmetry assumptions and characterized by normal coordinate analysis at the same level of theory.

**Table 1**  
Crystallographic data for **1–7** crystals.

	<b>1</b>	<b>2</b>	<b>3</b>	<b>4</b>	<b>5</b>	<b>6</b>	<b>7</b>
Formula	$C_{39}H_{25}N_9Mg$	$C_{46}H_{36}N_{10}OMg$	$C_{88.5}H_{65.5}N_{19.5}OMg_2$	$C_{74}H_{52}N_{17}O_{2.5}S_{1.5}Mg_2$	$C_{32}H_{22}N_8OSMg$	$C_{10}H_{18}O_6Mg$	$C_{10}H_{12}O_2$
Mol. Weight	643.99	769.16	1466.72	1316.01	614.97	258.55	164.20
Temperature (K)	295(2)	295(2)	295(2)	295(2)	295(2)	295(2)	295(2)
Crystal system	Monoclinic	Monoclinic	Triclinic	Triclinic	Triclinic	Monoclinic	Triclinic
Space group	P 2 <sub>1</sub> /c (No. 14)	P 2 <sub>1</sub> /n (No. 14)	P $\bar{1}$ (No. 2)	P $\bar{1}$ (No. 2)	P $\bar{1}$ (No. 2)	P 2 <sub>1</sub> /c (No. 14)	P $\bar{1}$ (No. 2)
a (Å)	12.123(2)	12.202(1)	15.159(1)	12.2698(8)	9.4144(8)	10.981(2)	7.454(1)
b (Å)	16.138(3)	12.793(2)	15.657(2)	12.5644(11)	13.306(2)	5.359(1)	7.611(1)
c (Å)	17.7160(3)	24.684(3)	16.457(2)	22.854(2)	23.497(3)	11.172(2)	16.021(2)
$\alpha$ (°)	109.652(5)	91.16(1)	78.54(1)	97.12(1)	90.12(1)	106.43(1)	93.628(7)
$\beta$ (°)	3264.1(8)	3852.4(8)	73.830(11)	93.65(1)	91.40(1)	630.6(2)	95.514(9)
$\gamma$ (°)	4	4	77.608(12)	109.15(2)	107.07(2)	2	99.885(11)
V (Å <sup>3</sup> )	1.31 / 1.311	1.32 / 1.326	3623.7(7)	3282.1(6)	2812.8(7)	1.36 / 1.362	888.3(2)
Z	0.099	0.098	2	2	2	0.154	4
D <sub>obs</sub> /D <sub>calc</sub>	0.32 × 0.28 × 0.22	0.37 × 0.33 × 0.27	1.34/1.344	1.33/1.332	1.45/1.452	0.38 × 0.35 × 0.21	1.22/1.228
$\mu$ (mm <sup>-1</sup> )	54,785/7816 /	71,544/9884/ 7195	0.100	0.148	0.184	12,646/1631 /	0.084
Crystal size (mm <sup>3</sup> )	5988	0.0259	0.24 × 0.17 × 0.12	0.35 × 0.29 × 0.24	0.27 × 0.23 × 0.22	1462	0.29 × 0.22 × 0.21
Total/unique/	0.0205	0.0450	60,403/17,674/ 8891	71,925/16,314/9885	94,691/15,897/	0.0217	11,732/4238/
Observed refls	0.0602	0.1064	0.0756	0.0298	8006	0.0275	2266
R <sub>int</sub>	0.1622	1.001	0.0993	0.0594	0.0803	0.0706	0.0526
R [F <sup>2</sup> > 2 $\sigma$ (F <sup>2</sup> )] <sup>a</sup>	1.014	0.172, -0.165	0.1684	0.1535	0.0658	1.000	0.0546
wR [F <sup>2</sup> all refls] <sup>b</sup>	0.857, -0.373		0.938	1.001	0.1356	0.222, -0.113	0.1418
S			0.472, -0.353	1.152, -0.673	1.004		1.000
$\Delta\rho_{max}$ , $\Delta\rho_{min}$ (e $\cdot$ Å <sup>-3</sup> )					0.212, -0.282		0.148, -0.169

<sup>a</sup>  $R = \sum ||F_o| - |F_c|| / \sum F_o$ .

<sup>b</sup>  $wR = \{ \sum [w(F_o^2 - F_c^2)^2] / \sum wF_o^4 \}^{1/2}$ ;  $w^{-1} = \sigma^2(F_o^2) + (aP)^2 + (bP)$  where  $P = (F_o^2 + 2F_c^2)/3$ . The a and b parameters are 0.0787 and 1.5094 for **1**, 0.0408 and 0.9851 for **2**, 0.0001 and 0 for **3**, 0.0780 and 0.3441 for **4**, 0.0450 and 0.6273 for **5**, 0.0332 and 0.1353 for **6**, and 0.0350 and 0 for **7**.

### 3. Results and discussion

#### 3.1. Synthesis

All obtained crystals were synthesized by the means of solvothermal technique. Initially prepared as described elsewhere [19] crystalline MgPc was added to dry 3,4-lut (10 mL), degassed and sealed under reduced pressure in a glass ampoule and next the ampoule was thermally processed for two days at 160 °C and then it was cooled to room temperature. In the such process electropositive Mg center of MgPc interacts with the electronegative nitrogen of 3,4-lut leading to MgPc-derivative with the axial Mg ← N coordination bond. During the cooling process the formed MgPc(3,4-lut) complex crystallises yielding blue-violet well-developed single crystals (**1**). In order to gain insight into the nature of the interaction between the reacted molecules, the three-dimensional molecular electrostatic potential have been calculated. It is defined as  $V(r) = \sum_A (Z_A / (R_A - r)) - \int (\rho(r') / |r' - r|) dr'$ , where  $Z_A$  is the charge on nucleus A having a position vector  $R_A$  and the  $\rho(r')$  is the electronic density function of the molecule, and  $r'$  is the dummy integration variable [63,64]. The molecular electrostatic potential (MESP) is related to the electronic density in molecule and is a very useful tool in determining sites for electrophilic and nucleophilic reactions as well as for intermolecular interactions and organisation of molecules in solid-state [65–67]. The MESP maps are obtained on the basis of the DFT (B3LYP/6–31+G(d)) optimised geometries of the reacted molecules (Fig. 1) as well as for the reaction product molecules (Fig. 2). For MgPc molecule the 3D MESP map displays the electrophilic region near the Mg center on both sides of planar MgPc molecule and the nucleophilic regions near the four bridged azamethine nitrogen atoms (Fig. 1a). In addition less positive value of MESP than that near the Mg center and less negative value of MESP comparing to that of azamethine N atoms are observed on both side of planar MgPc across the extended  $18\pi$  electron conjugation in the Pc(2–) macrocycle. The 3D MESP map for 3,4-lut molecule displays the nucleophilic region near the ring N atom containing the lone electron pair on the  $sp^2$  orbital (Fig. 1b). Therefore the interaction between the MgPc and 3,4-lut molecules takes place between the

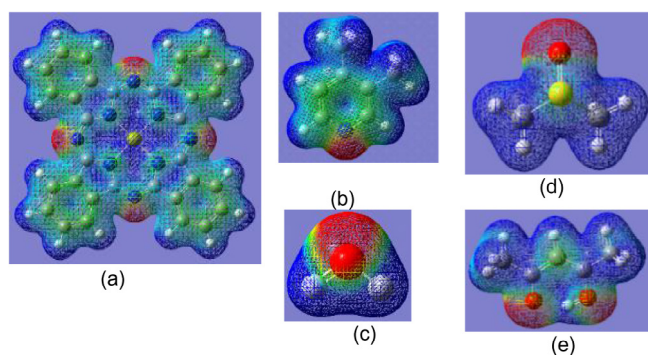


**Fig. 1.** 3D MESP for MgPc (a), 3,4-lutidine (b), H<sub>2</sub>O (c) DMSO (d) and acetylacetone (e). The colour code of MESP is in the range of  $-0.05$  (red) to  $0.05 \text{ e\AA}^{-1}$  (blue).

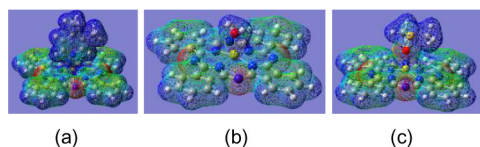


**Fig. 2.** 3D MESP for the MgPc(3,4-lut) (a), MgPc(H<sub>2</sub>O) (b) and MgPc(DMSO) (c). The colour code of MESP is in the range of  $-0.05$  (red) to  $0.05 \text{ e\AA}^{-1}$  (blue).

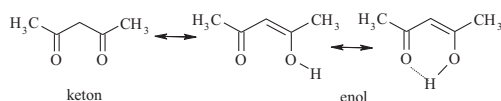
electropositive Mg center of MgPc and the ring N atoms of 3,4-lut, and in result the axial Mg ← N coordination bond is formed yielding the MgPc(3,4-lut) complex (**1**). The 3D MESP for the product is shown in Fig. 2a and will be helpful for understanding the interactions between the MgPc(3,4-lut) molecules during nucleation, crystallization and their organisation in solid-state.

The crystals of MgPc(H<sub>2</sub>O)·2(3,4-lut) (**2**) were obtained during solvothermal process of MgPc in the mixture of 3,4-lutidine and DMSO taken in the volume proportion of 10:1, whereas the crystals of [MgPc(3,4-lut)·(3,4-lut)][MgPc(H<sub>2</sub>O)·2(3,4-lut)]·½(3,4-lut) (**3**) and the crystals of [MgPc(H<sub>2</sub>O)·2(3,4-lut)][MgPc(DMSO)]·½(DMSO) (**4**) were obtained in the similar way as crystals **2**, however the volume ratio of 3,4-lutidine to DMSO was 5:1 and 1:1 in the case of crystals **3** and **4**, respectively. In all cases the reaction of MgPc in the respective 3,4-lut/DMSO system was thermally processed at 130 °C during two days. DMSO was added to the reaction mixtures in order to change the temperature dependence of the formed compounds solubility. It enabled to obtain the crystals of better quality. In the case of crystals **2** and **3** the DMSO moieties did not build into the crystal structures of obtained compounds. However, in the crystals **4** that were formed in the 3,4-lut/DMSO system with a greater amounts of DMSO (1:1), the DMSO molecules did build into the crystal structure. Since the MgPc is unstable in the air atmosphere due to its high affinity to moisture of air [20,22], the formed crystals contain water molecules. The high affinity of MgPc to water results from the interaction of lone pair of electron at oxygen atom of water molecule with electropositive Mg atom ( $\sim +0.5$ ) of MgPc, what is confirmed by the molecular orbital calculations [68]. The 3D MESP maps are helpful for understanding of the high affinity of MgPc to water and the formation in used reaction conditions of the aquamagnesium phthalocyanine complex (Figs. 1 and 2). The interaction of MgPc with the solvent molecules in the 3,4-lut/DMSO system takes place between the positively polarised Mg center of MgPc and the negatively polarised fragment of the respective solvent molecules. In the reaction with a small amounts of DMSO (as in the case of **2** and **3**) the water molecule as the smaller and with the greater mobility molecule comparing with the 3,4-lut and DMSO molecules participate in the reaction with MgPc forming MgPc(H<sub>2</sub>O) that crystallises with 3,4-lut as solvent molecules forming respective crystals **2** and **3**, whereas in the case of the greater amounts of DMSO in the system the competition between the solvent molecules in the interaction with MgPc takes place resulting in the formation of MgPc(H<sub>2</sub>O) and MgPc(DMSO) complexes that co-crystallise forming solvated crystals **4**. The interaction of electropositively polarised Mg center of MgPc in the 3,4-lut/DMSO/H<sub>2</sub>O takes place between the negatively polarised nucleophilic O atoms of water or DMSO and the ring N-atom of 3,4-lut molecules (Figs. 1 and 2). However, the Mg<sup>2+</sup> of MgPc molecule as a hard acid prefers the O as a harder base than N [69–71] forming MgPc(H<sub>2</sub>O) and MgPc(DMSO) complexes. The 3,4-lut present in the reaction system interacts with the formed MgPc(H<sub>2</sub>O) complex as an acceptor in the O–H···N hydrogen bonds forming depending on the crystallization conditions respective crystals **2**, **3** and **4**. The axial ligation of the Mg center of MgPc molecule and formation of MgPc(3,4-lut) complex (**1**) takes place only in the case of extremely conditions, using freshly obtained MgPc and dried 3,4-lutidine. The possibility of the formation of the MgPc(DMSO) complex in the mixture of 3,4-lut/DMSO taken in volume ratio of 1:1 that co-crystallise with the formed MgPc(H<sub>2</sub>O) forming crystals **4** induced us to perform the reaction of MgPc in pure DMSO. Since the boiling point of DMSO is  $\sim 189$  °C the solvothermal reaction of MgPc with DMSO was performed at 170 °C. At this temperature with a time the MgPc dissolved completely forming homogenous solution. During the cooling process the formed MgPc(DMSO) complex crystallises forming well-developed suitable for the X-ray analysis single crystals of **5**.

The **1–5** crystals are well soluble in 3,4-lutidine yielding intensively blue solutions. In ambient air, in solution in 3,4-*lut* the MgPc (3,4-*lut*) complex (**1**) transforms into MgPc(H<sub>2</sub>O) complex, and after several days it crystallises yielding MgPc(H<sub>2</sub>O)<sub>2</sub>(3,4-*lut*) (**2**). All **1–5** crystals are well soluble in pyridine, DMSO, DMF and other N- and O-donor solvents. The solubility of these **1–5** complexes are several times greater than the parent MgPc pigment due to the steric axial hindrance that lowers the  $\pi$ - $\pi$  stacking interactions in solid.

Solvothermal reaction of MgPc with 3,4-lutidine/acacH was performed at 120 °C. Next the homogenous solution was cooled to room temperature and left at the ambient conditions. After several days well-developed rectangular colourless single crystals of **6** appeared (Scheme 1).

It is well known that acetylacetone exists in two tautomeric forms in a dynamic equilibrium



Experimental and theoretical investigations of keto-enol tautomerization of acacH show that the enolic form of acacH with the internal O—H...O hydrogen bond is energetically favourable due to delocalisation of the  $\pi$ -electrons of the double C=C and C=O bonds and the lone pair of electron of the O atom forming six-membered ring with an aromatic character [72]. The equilibrium constant of the dissociation of the enol form of acacH ( $\text{acacH} \leftrightarrow \text{acac}^- + \text{H}^+$ ) strongly depends on the ionic strength, the solvent and the thermal conditions. The pKa in aqueous solution and with the ionic strength close to 0 is equal to 8.99 [73]. The electropositive Mg atom of MgPc molecule, which as shows single crystal analysis is non-planar [19], is significantly displaced from the N<sub>4</sub>-isoindole plane of Pc (~0.5 Å), therefore in such conditions in 3,4-*lut*/acacH solution it interacts with the formed acac<sup>-</sup> anions. The interaction of MgPc with acac<sup>-</sup> anions in 3,4-*lut*/acacH system could be better understood if we take into consideration the 3D MESP maps of reacted units (Fig. 3). The interaction of MgPc with

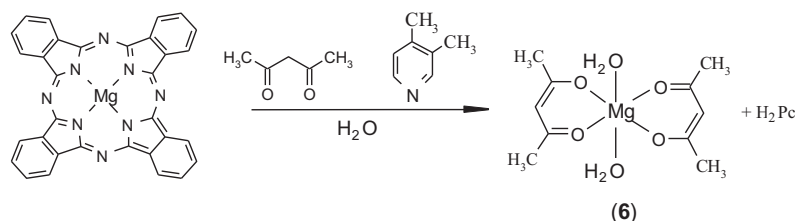
acac<sup>-</sup> in result interrupts the Mg—N bonds and leads to demetallation of MgPc and formation of the Mg(acac)<sub>2</sub> complex that in presence of the water molecules forms crystalline biaxially ligated by H<sub>2</sub>O [Mg(acac)<sub>2</sub>(H<sub>2</sub>O)<sub>2</sub>] complex (**6**) and metal-free phthalocyanine (H<sub>2</sub>Pc). The formed Mg(acac)<sub>2</sub>(H<sub>2</sub>O)<sub>2</sub> complex (**6**) crystallises as colourless rectangular well-developed suitable for the X-ray analysis crystals which after several days disappeared (i.e. underwent dissolving in parent solution). After three consecutive weeks in the mother liquor new colourless crystals **7** with other shapes comparing to crystals **6** appeared. The single crystal analysis of needle crystal **7** showed that it is a crystal of organic compound with a composition of C<sub>10</sub>H<sub>12</sub>O<sub>2</sub>, which along with the time is formed at ambient air in the mother liquor from compound **6**.

### 3.2. Thermal properties

In order to determine the thermal stability of the MgPc-derivatives, the thermal analyses of **1–5** were carried out on the samples of 15–20 mg with the same heating rate of 5 °C/min. Crystals of **1** are stable up to ~100 °C (Fig. S1 in Supplementary). The mass loss is concerned with the release of 3,4-*lut* from the MgPc(3,4-*lut*) complex and above ~120 °C the rest of the sample gives free MgPc in the  $\beta$ -form that was confirmed by the X-ray powder diffraction experiment. The respective mass loss on the heating is ~16.5 and is in agreement with the calculated value of 16.64% (loss of 3,4-*lut*).

The crystals of **2** are stable up to ~100 °C (Fig. S2) and at higher temperature they lose both solvated 3,4-*lut* molecules transforming into aquamagnesium phthalocyanine (MgPcH<sub>2</sub>O) that loses the coordinated water molecule above 200 °C, which is in agreement with that of the thermal decomposition of the triclinic modification of aquamagnesium phthalocyanine complex [22]. The respective mass losses on the heating of ~27.8 and ~30.1% are in agreement with the calculated values of 27.86% (3,4-*lut*) and 30.20% (total mass of 3,4-*lut* and H<sub>2</sub>O).

The thermogravimetric analysis of the crystals of **3** shows their less-stability (Fig. S3). At ~90 °C the sample of crystals **3** releasing the solvated 3,4-*lut* molecules and then coordinated (at ~125), transforms into MgPc(H<sub>2</sub>O) complex that loses the coordinated water at ~200 °C. The respective mass losses on the heating are 18.5, 25.5 and 26.7% are in agreement with the calculated values



Scheme 1. Formation of the Mg(acac)<sub>2</sub>(H<sub>2</sub>O)<sub>2</sub> complex (**6**).

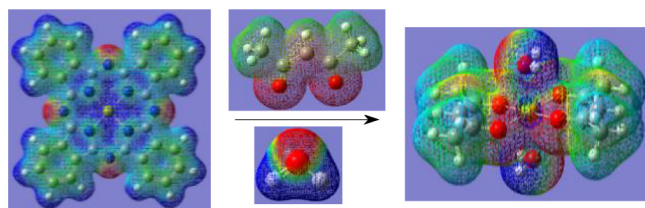


Fig. 3. 3D MESP for MgPc, acac<sup>-</sup>, H<sub>2</sub>O and for the Mg(acac)<sub>2</sub>(H<sub>2</sub>O)<sub>2</sub>. The colour code of MESP is in the range of -0.05 (red) to 0.05 e<sup>-1</sup> (blue).

of 18.26% (loss of solvated 3,4-*lut*), 25.57% (solvated + coordinated 3,4-*lut*) and 26.80% (solvated + coordinated 3,4-*lut* + coordinated H<sub>2</sub>O). Finally the sample transforms into MgPc in the  $\beta$ -form.

During the heating process the crystals **4** gradually undergo decomposition (Fig. S4). Crystals **4** are stable up to  $\sim 80^\circ\text{C}$ , which is the first step of the mass loss. The mass loss is concerned with the release of disordered DMSO molecule. The second step of the mass loss (at  $\sim 145\text{--}150^\circ\text{C}$ ) is concerned with the release of solvated 3,4-*lut* molecule and the third is concerned with the release of coordinated water molecule and finally at  $\sim 245\text{--}250^\circ\text{C}$  the mass loss is concerned with the release of coordinated DMSO molecule. The respective mass losses on the heating are  $\sim 2.90$ , 11.0, 12.5 and 18.41%, and are in agreement with the calculated values of 2.97% (loss of disordered DMSO), 11.51% (loss of disordered DMSO and 3,4-*lut* molecules), 12.47% (loss of disordered DMSO, 3,4-*lut* and coordinated water molecules) and 18.41% (loss of disordered DMSO, 3,4-*lut* and coordinated water and DMS molecules). TG analysis of **4** is in agreement with their composition of  $\{[\text{MgPc}(\text{H}_2\text{O}) \cdot (3,4\text{-lut})][\text{MgPc}(\text{DMSO})] \cdot \frac{1}{2}(\text{DMSO})\}$  and points on the higher thermal stability of MgPc(DMSO) than MgPc(H<sub>2</sub>O).

The thermal stability of the complex **5** has been also determined (Fig. S5). During the heating process compound **5** is stable up to  $\sim 225^\circ\text{C}$  and at higher temperature it loses axial DMSO molecule and transforms into MgPc in the  $\beta$ -form. The mass loss on the heating of 12.8% is in agreement with the calculated value of 12.71% that is concerned with the release of coordinated DMSO molecule.

### 3.3. Description of the crystal structures of magnesium phthalocyanine derivatives

#### 3.3.1. MgPc(3,4-*lut*) complex (**1**)

Compound **1** crystallises in the centrosymmetric space group  $P2_1/c$  of the monoclinic system. The molecular structure of MgPc(3,4-*lut*) complex is illustrated in Fig. 4a. In contrast to the complexes obtained in dry pyridine (MgPc(py)<sub>2</sub>) [30] and in dry 3,5-lutidine (MgPc(3,5-*lut*)<sub>2</sub>) [52], both exhibit 4 + 2 coordination environment of Mg, the complex **1** exhibits 4 + 1 square pyramidal coordination environment of Mg. The interaction of the electropositively polarised Mg center of MgPc with electronegatively polarised ring N atom of the axial 3,4-*lut* molecule results in displacement of the Mg atom from the N<sub>4</sub>-isonodole plane of phthalocyaninate(2-) macrocycle that adopts a saucer-shape form. The displacement of Mg from the N<sub>4</sub>-plane of 0.534(2) Å is comparable to that of  $\sim 0.5$  Å in the crystal of MgPc, in which the displacement of Mg from MgPc plane results from the intermolecular interaction between the Mg center of one MgPc molecule with the *N*-azamethine nitrogen atom of the neighbour [19]. The monoaxial ligation of Mg center of MgPc by the *N*-donor ligands is relatively rare in relation to ligation by O-donor ligand. The monoaxial ligation of Mg center of MgPc by *N*-donor ligand can be found in the crystal of MgPc-derivative with the axial ligand of 2-amino-3-picoline [74], in which the displacement of Mg from N<sub>4</sub>-isonodole plane of 0.498(3) Å is similar to that observed in **1**. The plane of the 3,4-*lut* molecule is almost perpendicular to the N<sub>4</sub>-plane of Pc(2-) macrocycle. The orientation of the planar axial ligand relative to the phthalocyaninato(2-) macrocycle is determined by the electrostatic interaction between the electropositively polarised H atoms in *orto* positions in relation to *N*-ring atom of 3,4-*lut* and the electronegatively polarised azamethine nitrogen atoms of Pc(2-) macrocycle (Figs. 1 and 2). This conformation of MgPc(3,4-*lut*) complex is the most stable and is preferred in solution and in the gas-phase as is evidenced by the DFT molecular orbital calculations. The coordination polyhedron around the Mg cation approximates to a tetragonal pyramid with relatively long bond between the Mg and the N atom of the axial 3,4-*lut* ligand. The four

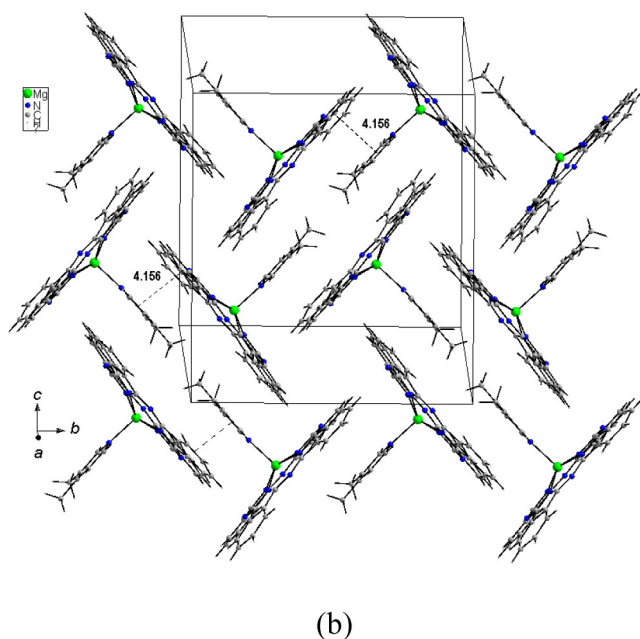
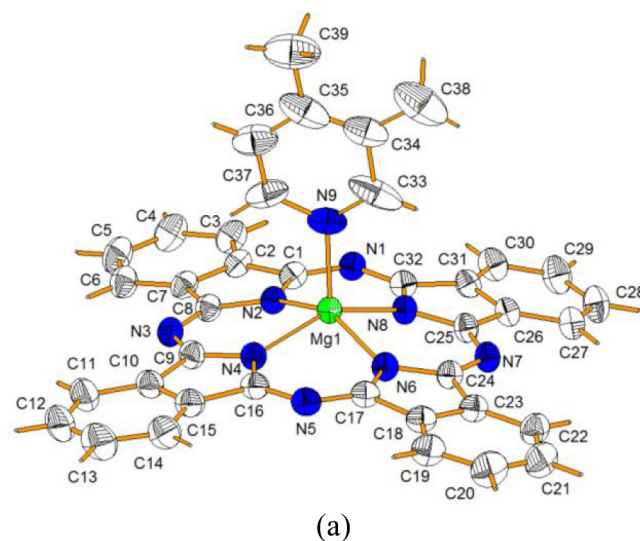


Fig. 4. View of the molecular structure of **1** along with the labelling scheme (a) and the crystal packing of **1** (b). Thermal ellipsoids are shown at the 50% probability level, H atoms with arbitrary radii.

equatorial Mg–N bonds with the Pc(2-) macrocycle are significantly shorter ( $\sim 0.8$  Å) than the axial Mg–N bond linking the 3,4-*lut* ligand (Table 2). DFT geometry optimisation of the MgPc(3,4-*lut*) molecule yields similar conformation as present in the crystal. However, looking in more details on the DFT geometrical parameters it should be stated that the greatest discrepancy between the X-ray and theoretical values is found in the axial Mg–N bond. The theoretical value of the axial Mg–N bond is longer by  $\sim 0.08$  Å than the X-ray value. Quite similar correlation between the X-ray and DFT values of the equatorial Mg–N bond was observed in other MgPc complexes axially ligated by pyridine and imidazole, MgPc(py) and MgPc(Im) [75]. Full geometrical parameters of the optimised conformation of the MgPc(3,4-*lut*) molecule are listed

**Table 2**  
Selected geometrical parameter for MgPc(3,4-lut) molecule in crystals **1** and **3**.

	(1)	(3)	DFT	
Mg1–N2	2.0435(16)	Mg2–N10	2.061(4)	2.058
Mg1–N4	2.0467(16)	Mg2–N12	2.034(4)	2.058
Mg1–N6	2.0487(16)	Mg2–N14	2.047(4)	2.059
Mg1–N8	2.0470(16)	Mg2–N16	2.037(4)	2.059
Mg1–N9	2.127(2)	Mg2–N17	2.153(4)	2.209
N2–Mg1–N4	86.35(6)	N10–Mg2–N12	85.77(16)	86.8
N4–Mg1–N6	85.88(6)	N12–Mg2–N14	86.57(16)	87.2
N6–Mg1–N8	86.30(6)	N14–Mg2–N16	86.65(17)	87.2
N8–Mg1–N2	85.94(6)	N16–Mg2–N10	86.43(17)	86.9
N9–Mg1–N2	105.86(8)	N17–Mg2–N10	101.68(16)	103.1
N9–Mg1–N4	101.72(8)	N17–Mg2–N12	102.94(17)	103.1
N9–Mg1–N6	104.51(8)	N17–Mg2–N14	107.41(17)	103.3
N9–Mg1–N8	108.19(9)	N17–Mg2–N16	106.31(16)	103.3
N2–Mg1–N9–C37	48.8(2)	N10–Mg2–N17–C69	50.6(3)	44.8
Deviation of Mg from the N <sub>4</sub> -plane	0.534(2)		0.516(3)	0.470

in Supplementary (Table S1). The arrangement of MgPc(3,4-lut) molecules in the crystal is mainly determined by the van der Waals forces and the electrostatic interactions between the molecules (Fig. 4b), since the steric hindrance of the axial 3,4-lut ligand significantly reduces the  $\pi$ – $\pi$  interactions between phthalocyaninato (2–) macrocycles as observed in the crystal of unhindered parent MgPc [19]. The closest interplanar distance of  $\sim 4.15$  Å between neighbouring MgPc(3,4-lut) molecules can be found between the Pc(2–) macrocycle of one molecule and the plane of the axial 3,4-lut ligand of the neighbours (Fig. 4b). In addition the characteristic feature of the compound **1** crystal structure is the lack of the  $\pi$ – $\pi$  interactions between phthalocyaninato(2–) macrocycles. Thus, the architecture of MgPc(3,4-lut) crystals is less stabilised by the  $\pi$ – $\pi$  interactions. This is manifested in the increasing of the MgPc(3,4-lut) solubility in the most common solvents and improved technical performance of the pigment.

### 3.3.2. MgPc(H<sub>2</sub>O)·2(3,4-lut) complex (**2**)

Compound **2** crystallises in the centrosymmetric space group  $P2_1/n$  of the monoclinic system with four molecules per unit cell. Asymmetric unit of **2** consists of one MgPc(H<sub>2</sub>O) moiety and two 3,4-lut molecules linked together via O–H...N hydrogen bonds (Fig. 5a). The Mg atom of MgPc(H<sub>2</sub>O) molecule exhibits tetragonal–pyramidal environment (4 + 1 coordination) and is deviated from the average plane defined by four isoindole N atoms by 0.464(2) Å toward the oxygen atom of water molecule. The displacement of Mg from the N<sub>4</sub>-plane is comparable to that observed for the monoclinic and triclinic modifications of aquamagnesium phthalocyanine [22,76,77], and is higher by  $\sim 0.2$  Å than that in some chlorophyll derivatives [78,79]. The axial Mg–O bond is somewhat shorter than the equatorial four Mg–N bonds linked the phthalocyaninato(2–) macrocycle (Table 3). Quite similar tetragonal–pyramidal environment of Mg atom of MgPc(H<sub>2</sub>O) complex is preferred in solution and in the gas-phase as is evidenced by the DFT molecular orbital calculations, however the opposite relation between the values of the axial Mg–O and equatorial Mg–N bonds is observed. The theoretical DFT value of the axial Mg–O bond is longer by  $\sim 0.12$  Å than the X-ray value (Table 3). Full geometrical parameters of the optimised conformation of the MgPc(H<sub>2</sub>O) molecule are listed in Supplementary (Table S2). The solvated 3,4-lut molecules lie in different planes. One of them that contains the N9 atom is inclined to the N<sub>4</sub>-isoindole plane by 21.3(1)°, whereas the other 3,4-lut with the N10 atom is inclined by 56.2(1)°. Both H atoms of coordinated water molecule take part in the almost linear hydrogen bonds with N pyridine atoms of solvation 3,4-lut molecules. The geometry of both O–H...N hydrogen

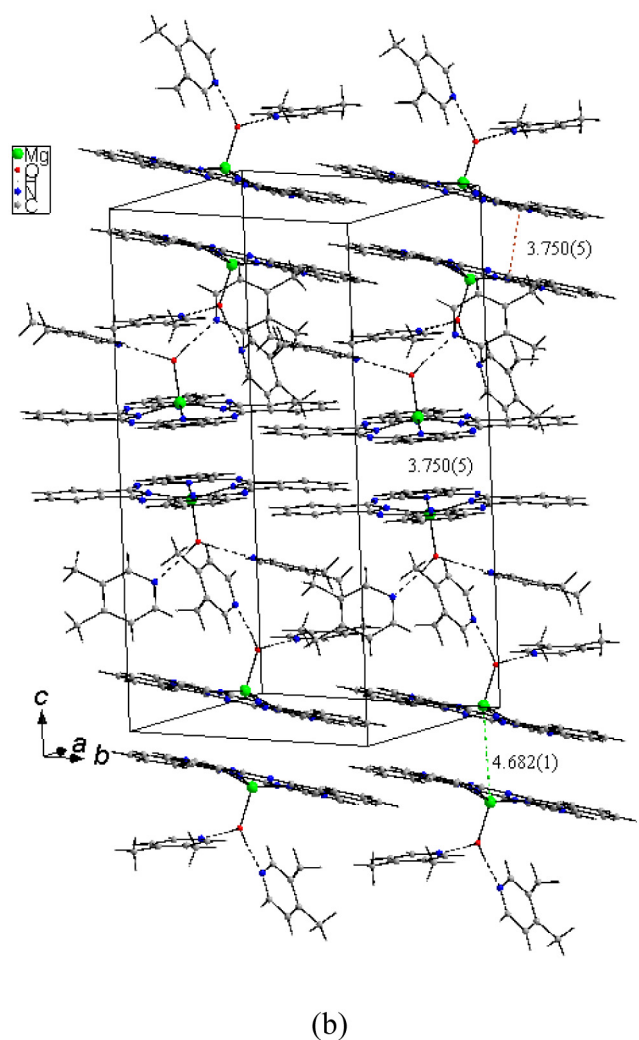
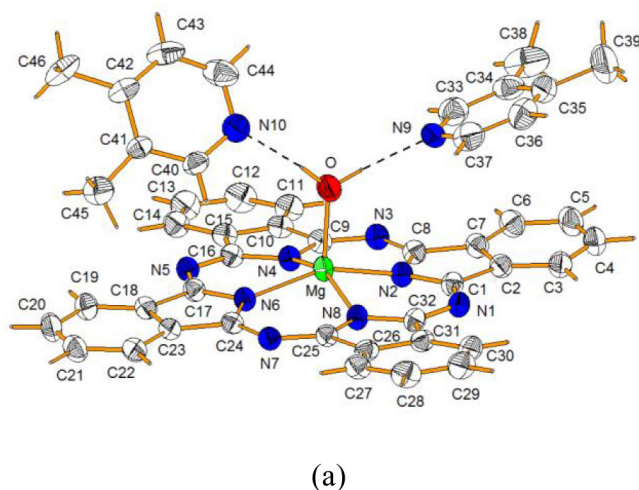


**Fig. 5.** View of the molecular structure of **2** along with the labelling scheme (a) and the crystal packing showing the Mg...Mg and N<sub>4</sub>...N<sub>4</sub> distances between the back-to-back units of **2** (b). Thermal ellipsoids are shown at the 50% probability level, H atoms with arbitrary radii.

bonds linking the solvation 3,4-lut molecules is quite similar (Table 4). Arrangement of MgPc(H<sub>2</sub>O)·2(3,4-lut) units in the crystal is mainly determined by the van der Waals forces and by the  $\pi$ – $\pi$  interactions. However, due to the steric hindrance of axial water

**Table 3**  
Selected geometrical parameters (Å, °) for MgPc(H<sub>2</sub>O)·2(3,4-*lut*) in crystals **2**, **3** and **4**.

	(2)	(3)	(4)	DFT
Mg1–N2	2.0351(11)	2.049(4)	2.0488(16)	2.040
Mg1–N4	2.0361(11)	2.034(4)	2.0511(17)	2.043
Mg1–N6	2.0348(11)	2.056(4)	2.0533(16)	2.040
Mg1–N8	2.0402(11)	2.035(4)	2.0489(16)	2.043
Mg1–O1	2.0028(12)	1.990(4)	2.0227(17)	2.146
N2–Mg1–N4	87.24(4)	85.93(15)	87.40(7)	88.1
N4–Mg1–N6	87.03(4)	86.44(16)	85.61(7)	88.1
N6–Mg1–N8	87.10(4)	85.16(16)	87.85(6)	88.1
N8–Mg1–N2	86.75(4)	86.20(15)	85.67(6)	88.1
O1–Mg1–N2	98.68(5)	103.02(15)	102.13(7)	99.9
O1–Mg1–N4	103.05(5)	108.97(18)	107.83(7)	101.1
O1–Mg1–N6	106.83(5)	107.12(16)	105.92(7)	99.9
O1–Mg1–N8	104.02(5)	102.62(18)	100.16(7)	101.1
Deviation of Mg from the N <sub>4</sub> -plane	0.464(2)	0.544(3)	0.497(2)	0.470
Dihedral angle between the planes of N <sub>4</sub> and 3,4- <i>lut</i>				
N <sub>4</sub> /N9	21.3(1)	N <sub>4</sub> /N18	11.2(1)	
N <sub>4</sub> /N10	56.2(1)	N <sub>4</sub> /N19	69.3(1)	N <sub>4</sub> /N17 71.0(1)

**Table 4**  
Hydrogen-bond geometry (Å, °) in **2**.

D–H...A	D–H	H...A	D...A	D–H...A
O1–H2O...N9	0.88(2)	1.84(2)	2.7270(18)	176.3(18)
O1–H10...N10	0.86(2)	1.91(2)	2.7715(19)	174.2(19)

molecule together with the linking the solvation 3,4-*lut* molecules, as well as the deformation of Pc<sup>2-</sup> macrocycle, the  $\pi$ – $\pi$  interactions between the molecules in the crystal **2** are significantly weaker when comparing to parent MgPc pigment with the  $\pi$ – $\pi$  stacking interactions [19]. Inversion related MgPc(H<sub>2</sub>O)·2(3,4-*lut*) units are arranged in the back-to-back fashion with a distance of ~3.75 Å between the saucer-shaped phthalocyaninato(2-) macrocycles (Fig. 5b).

### 3.3.3. [MgPc(3,4-*lut*)] [MgPc(H<sub>2</sub>O)·2(3,4-*lut*)]·½(3,4-*lut*) – (3)

Compound **3** crystallises in the centrosymmetric space group of the triclinic system. Asymmetric unit of **3** is built of one molecule of MgPc(3,4-*lut*) and one MgPc(H<sub>2</sub>O)·2(3,4-*lut*) moiety and half of 3,4-*lut* molecule (Fig. 6a). Both compounds, MgPc(3,4-*lut*) and MgPc(H<sub>2</sub>O)·2(3,4-*lut*), co-crystallise with 3,4-*lut* as solvent that in the crystal is disordered. The disordered solvent 3,4-*lut* molecule lies in the inversion center, so it has two orientation. The conformation of the MgPc(3,4-*lut*) and MgPc(H<sub>2</sub>O)·2(3,4-*lut*) moieties in crystal **3**, in general, similar to that found for the respective complexes in the crystal **1** and **2** and comparable to that in the gas-phase as is evidenced by the DFT molecular orbital calculations (Tables S1 and S2). However, small differences in the bond lengths and angles in the MgPc(3,4-*lut*) molecule in the crystal **3** and crystal **1** are observed (Table 2). The orientation of the planar axial 3,4-*lut* ligand relative to the phthalocyaninato(2-) macrocycle in the crystal **3** is similar to that in the crystal **1** that results from the electrostatic interaction between the electropositively polarised H atoms in *orto* positions in relation to N-ring atom of 3,4-*lut* and the electronegatively polarised azamethine nitrogen atoms of Pc(2-) macrocycle. Small differences between the geometrical parameters of the coordination sphere of Mg the in MgPc(H<sub>2</sub>O)·2(3,4-*lut*) moiety in the crystal **3** and **2** are also observed (Table 3). These differences result from the intermolecular interactions present in the crystals. The orientation of the hydrogen bonded 3,4-*lut* molecules in the MgPc(H<sub>2</sub>O)·2(3,4-*lut*) moiety in the crystal **3** is slightly different than that in the crystal **2**. One of them that contains the N18 atom is less inclined (11.2(2)°) and the other 3,4-*lut* with the N19 atom is more inclined (69.3(2)°) to the N<sub>4</sub>-isoindole

plane of Pc<sup>2-</sup> macrocycle when comparing to the respective values in the crystal **2** (Table 3). The different orientation of both hydrogen bonded 3,4-*lut* molecules in the MgPc(H<sub>2</sub>O)·2(3,4-*lut*) moiety in **3** in relation to **2** results in the slight change of the geometry of hydrogen bonds (Tables 4 and 5). The planar ring of disordered solvent 3,4-*lut* molecule located in the inversion center is almost parallel to the average plane of Pc<sup>2-</sup> macrocycle of MgPc(3,4-*lut*) (dihedral angle between N<sub>4</sub>-plane of Pc<sup>2-</sup> and the plane of the disordered 3,4-*lut* molecule is equal to 19.7(3)°), whereas is almost perpendicular the average plane of Pc<sup>2-</sup> macrocycle of MgPc(H<sub>2</sub>O) (dihedral angle is equal to 83.0(3)°). Arrangement of the MgPc(3,4-*lut*) and MgPc(H<sub>2</sub>O)·2(3,4-*lut*) moieties together with the disordered solvent 3,4-*lut* molecule in **3** is mainly determined by the van der Waals forces, electrostatic and by the  $\pi$ – $\pi$  interactions. Related by inversion MgPc(3,4-*lut*) molecules form dimers in the back-to-back fashion with a distance of 3.634(3) Å between the N<sub>4</sub>-planes of Pc<sup>2-</sup> macrocycles. However, the distance between the average planes of Pc<sup>2-</sup> macrocycles is shorter by ~0.2 Å due to the saucer-shaped form pointing on the  $\pi$ – $\pi$  interactions between the  $\pi$ -clouds of phthalocyaninato(2-) macrocycles. The inversion related MgPc(H<sub>2</sub>O)·2(3,4-*lut*) moieties are also oriented in the back-to-back fashion, however the distance between the N<sub>4</sub>-planes of Pc<sup>2-</sup> macrocycles is much greater (7.264(5) Å) since the Pc<sup>2-</sup> macrocycles interpenetrates the 3,4-*lut* of neighbouring MgPc(3,4-*lut*) molecules (Fig. 6b). The average planes of phthalocyaninato(2-) macrocycles of the back-to-back inversion related MgPc(H<sub>2</sub>O)·2(3,4-*lut*) moieties and back-to-back inversion related MgPc(3,4-*lut*) molecules are respectively almost parallel and perpendicular to (1 0 0) crystallographic plane. The steric hindrance of axial ligands and the deformation of phthalocyaninato(2-) macrocycle of both MgPc(3,4-*lut*) and MgPc(H<sub>2</sub>O)·2(3,4-*lut*) moieties in **3** makes them more sensitive for action of solvents and is responsible for the increase in their solubility.

### 3.3.4. [MgPc(H<sub>2</sub>O)·(3,4-*lut*)] [MgPc(DMSO)]·½(DMSO) – (4)

Compound **4** crystallises in the centrosymmetric space group of the triclinic system. Asymmetric unit of **4** is built of one MgPc(DMSO) and one MgPc(H<sub>2</sub>O) molecules that co-crystallise with

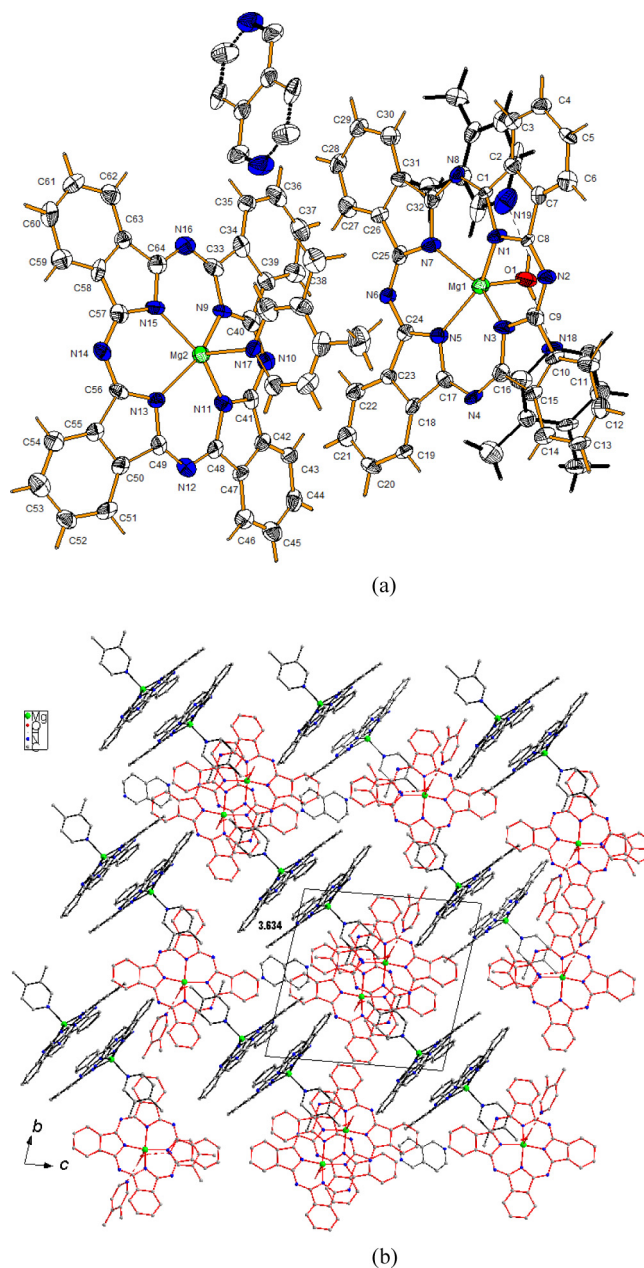


**Fig. 6.** View of the molecular structure of **3** along with the labelling scheme, thermal ellipsoids are shown at the 50% probability level, H atoms with arbitrary radii (a) and the crystal packing showing the  $N_4-N_4$  distances between the back-to-back units of **3**, the  $MgPc(3,4-lut)$  and  $MgPc(H_2O)_2(3,4-lut)$  units are shown in black and red, respectively (b).

**Table 5**  
Hydrogen-bond geometry ( $\text{\AA},^\circ$ ) in **3**.

$D-H\cdots A$	$D-H$	$H\cdots A$	$D\cdots A$	$D-H\cdots A$
$O1-H10\cdots N18$	0.82(1)	1.91(1)	2.727(4)	175(5)
$O1-H2O\cdots N19$	0.82(1)	2.08(1)	2.844(7)	154(2)

*3,4-lut* and half disordered DMSO as solvent molecules (Fig. 7a). The solvation *3,4-lut* molecule is linked together with  $MgPc(H_2O)$  via  $O-H\cdots N$  hydrogen bond. The coordination of Mg atom in both  $MgPc$ -complexes is characterised by the tetragonal-pyramidal environment of four equatorial *N*-isoindole atoms of phthalocyanine ring and the oxygen atom of axially coordinated water or

DMSO molecules. Interaction of electropositively polarised Mg atom of  $MgPc$  molecule with electronegatively polarised O atom of DMSO and water molecules leads to its displacement from the mean plane of four *N*-isoindole atoms by 0.497(2) and 0.474(2)  $\text{\AA}$  in direction of oxygen atom of water and DMSO molecules, respectively. In addition, the interaction of Mg and the O atoms results in deviation of a planar phthalocyaninato(2-) macrocycle in a saucer-shape form. The geometrical parameters of the  $MgPc(H_2O)$  molecule in crystal **4** are quite similar to that observed in the crystals **2** and **3** (see Table 3), whereas that in  $MgPc(DMSO)$  molecule are listed in Table 6. The X-ray geometrical parameters of the coordination environment of Mg cation in both axially ligated by O  $MgPc$  molecules,  $MgPc(DMSO)$  and  $MgPc(H_2O)$ , are quite similar, i.e. the axial  $Mg-O$  bond is shorter than the four equatorial  $Mg-N$  bonds.

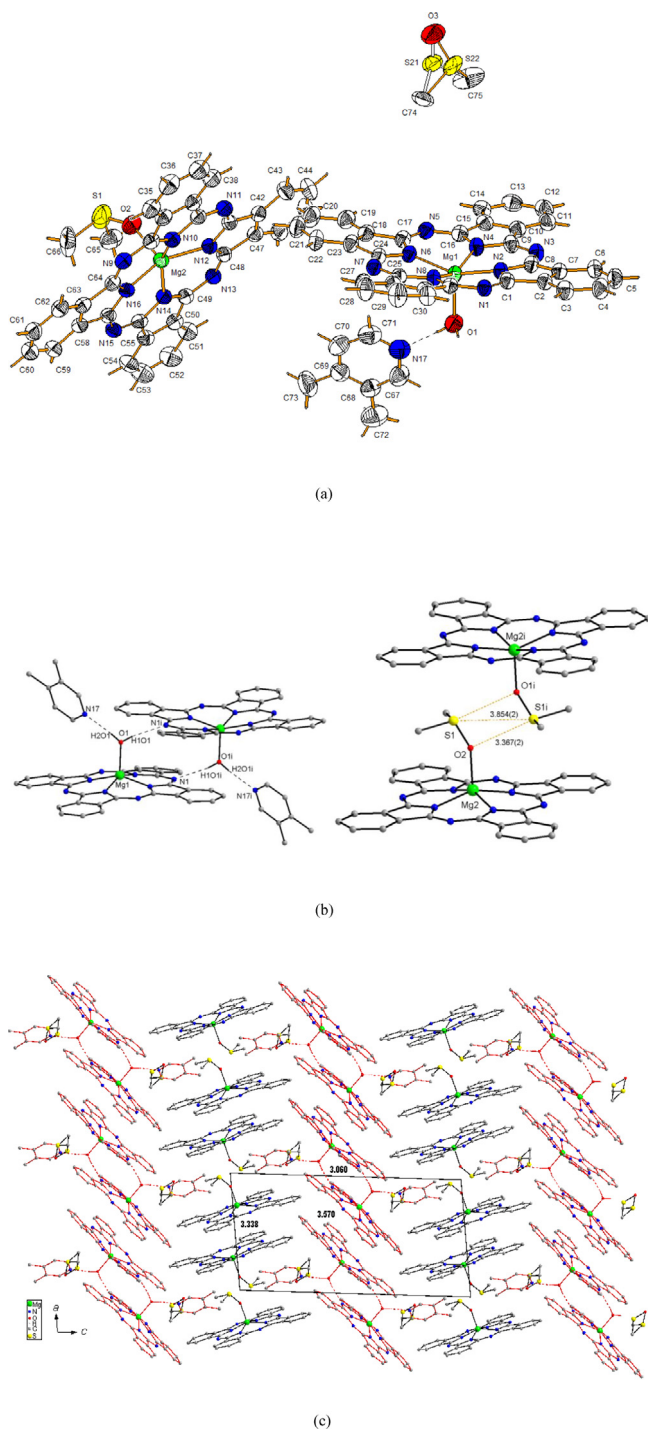


**Fig. 7.** View of the molecular structure of **4** along with the labelling scheme, thermal ellipsoids are shown at the 50% probability level, H atoms with arbitrary radii (a) and the face to face dimers of  $[(\text{MgPc}(\text{H}_2\text{O})\cdot(3,4\text{-lut}))_2]$  and  $[\text{MgPc}(\text{DMSO})_2]$  (b) and the crystal packing showing the  $\text{N}_4\text{-N}_4$  distances between the back-to-back units in **4**, the  $[(\text{MgPc}(\text{H}_2\text{O})\cdot(3,4\text{-lut}))_2]$  and  $[\text{MgPc}(\text{DMSO})_2]$  units are shown in red and black, respectively (c).

In general, the DFT theoretical parameters agree well with the X-ray values, however the DFT axial Mg–O bond of the  $\text{MgPc}(\text{H}_2\text{O})$  molecule is longer than the four equatorial Mg–N bonds, but in the  $\text{MgPc}(\text{DMSO})$  molecule the axial Mg–O bond is somewhat shorter than the four equatorial Mg–N bonds. The Mg–O binding strength in  $\text{MgPc}(\text{DMSO})$  and  $\text{MgPc}(\text{H}_2\text{O})$  molecules is related to properties of the ligands such as basicity and the Gutmann donor number

[80,81]. The  $\text{MgPc}(\text{H}_2\text{O})$  molecule links the solvent 3,4-*lut* molecule via  $\text{O}-\text{H}\cdots\text{N}$  hydrogen bond (Table 7). The orientation of the hydrogen bonded 3,4-*lut* molecule in the  $\text{MgPc}(\text{H}_2\text{O})\cdot(3,4\text{-lut})$  moiety in the crystal **4** is inclined to the  $\text{N}_4$ -plane of  $\text{Pc}^{2-}$  macrocycle by  $71.0(1)^\circ$ . In the crystal the  $\text{MgPc}(\text{H}_2\text{O})\cdot(3,4\text{-lut})$  and  $\text{MgPc}(\text{DMSO})$  molecules related by an inversion are forming face-to-face dimeric structures (Fig. 7b). The dimeric structure of  $[\text{MgPc}(\text{H}_2\text{O})\cdot(3,4\text{-lut})]_2$  is formed by  $\text{O}-\text{H}\cdots\text{N}$  hydrogen bond formed between the coordinated oxygen atom of water molecule as a donor of one molecule of  $\text{MgPc}(\text{H}_2\text{O})$  and the *N*-azamethine atom of the second one with relatively short interplanar  $\text{N}_4 - \text{N}_4$  distance of  $3.606(2)$  Å. The second dimeric structure of  $[\text{MgPc}(\text{DMSO})]_2$  is formed by  $\text{S}\cdots\text{S}$  and  $\text{S}\cdots\text{O}$  interactions between the face-to-face molecules related by inversion with relatively long interplanar  $\text{N}_4\cdots\text{N}_4$  distance of  $6.995(3)$  Å between the  $\text{Pc}^{2-}$  macrocycles. Both dimers of face-to-face oriented molecules of  $\text{MgPc}(\text{H}_2\text{O})\cdot(3,4\text{-lut})$  and  $\text{MgPc}(\text{DMSO})$  are arranged in a stacking structure along the *a*-axis (Fig. 7c). The  $\text{N}_4 - \text{N}_4$  distances between the back-to-back oriented phthalocyaninato(2-) macrocycles along the stacks of  $[\text{MgPc}(\text{H}_2\text{O})\cdot(3,4\text{-lut})]_2$  and  $[\text{MgPc}(\text{DMSO})]_2$  dimers are  $3.570(2)$  and  $3.338(2)$  Å, respectively. The dimers in **4** form highly ordered stacking structure, while the interstacking space is filled by the disordered DMSO solvent molecules (Fig. 7c). Thus the  $\pi$ - $\pi$  interaction between the  $\pi$ -clouds of phthalocyaninato(2-) macrocycles between the dimers is responsible for their organisation in solid, however due to the  $\text{Pc}^{2-}$  macrocyclic distortion from planar conformation, the  $\pi$ - $\pi$  interaction is less effective in comparison to that in the parent  $\text{MgPc}$  pigment. So their solubility is 4–5 times higher than  $\text{MgPc}$ .

### 3.3.5. $\text{MgPc}(\text{DMSO})$ complex – (5)

Compound **5** crystallises in the centrosymmetric space group of the triclinic system with four  $\text{MgPc}(\text{DMSO})$  molecules per unit cell. Asymmetric unit of **5** consists of two independent  $\text{MgPc}(\text{DMSO})$  molecules, in one of them the axial DMSO ligand is ordered whereas in the other the axial DMSO ligand exhibits two non-equivalent orientations with the occupation factors of  $0.706(2)$  and  $0.294(2)$  for S11 and S12, respectively (Fig. 8a). The coordination of Mg in both  $\text{MgPc}(\text{DMSO})$  molecules exhibits tetragonal-pyramidal environment of four equatorial *N*-isoindole atoms of  $\text{Pc}^{2-}$  macrocycle and oxygen atom of axially coordinated DMSO molecule. The four equatorial Mg–N bonds with the  $\text{Pc}^{2-}$  macrocycle are slightly longer than the axial Mg–O bond linked the DMSO molecule. Theoretical DFT optimisation of  $\text{MgPc}(\text{DMSO})$  molecule shows similar conformational parameters as in the crystal. The equatorial Mg–N and axial Mg–O bonds in the  $\text{MgPc}(\text{DMSO})$  molecule obtained by the DFT calculations exhibits similar correlation as found in the crystal, however the DFT axial Mg–O bond is somewhat longer than X-ray value, but still shorter than the equatorial Mg–N bonds (Table 6). Full geometrical parameters of the optimised conformation of the  $\text{MgPc}(\text{DMSO})$  molecule are listed in Supplementary (Table S3). The interaction of electropositively polarised Mg with electronegatively polarised O atom of DMSO ligand leads to its displacement for the  $\text{N}_4$ -isoindole plane by  $0.456(1)$  and  $0.445(1)$  Å in the  $\text{MgPc}(\text{DMSO})$  molecules with ordered and disordered axial ligand, respectively. This interaction results in deformation of the phthalocyaninate(–2) macrocycle from the planar conformation to the saucer-shape form. In the crystal **5**, both independent  $\text{MgPc}(\text{DMSO})$  molecules related by inversion are forming dimeric structures in the face-to-face fashion (Fig. 8b). The conformation of the  $[\text{MgPc}(\text{DMSO})]_2$  dimer with ordered axial DMSO ligand in crystal **5** is very similar to that in the crystal **4**, whereas the structure of  $[\text{MgPc}(\text{DMSO})]_2$  dimer with disordered axial DMSO ligand resembles the dimeric structure of  $[\text{MgPc}(\text{H}_2\text{O})\cdot(3,4\text{-lut})]_2$  observed in crystal **4** (see Figs. 7b and 8b). The interplanar  $\text{N}_4 - \text{N}_4$  distances are  $6.915(6)$  and  $3.691(3)$  Å in

**Table 6**  
Selected geometrical parameters ( $\text{\AA}$ ,  $^\circ$ ) for  $\text{MgPc}(\text{DMSO})$  complex in crystals **4** and **5**.

4			5		DFT
			Mol. A	Mol. B	
Mg2–N10	2.0413(16)	Mg1–N2	2.031(2)	2.034(2)	2.059
Mg2–N12	2.0392(16)	Mg1–N4	2.035(2)	2.033(2)	2.063
Mg2–N14	2.0343(16)	Mg1–N6	2.040(2)	2.030(2)	2.069
Mg2–N16	2.0418(16)	Mg1–N8	2.037(2)	2.026(2)	2.067
Mg2–O2	2.0014(16)	Mg1–O1	2.017(2)	2.005(2)	2.059
N10–Mg2–N12	86.72(7)	N2–Mg1–N4	87.27(8)	87.50(8)	86.7
N12–Mg2–N14	87.07(6)	N4–Mg1–N6	87.01(8)	86.79(8)	86.5
N14–Mg2–N16	86.74(6)	N6–Mg1–N8	86.58(8)	88.11(8)	86.4
N10–Mg2–N16	87.08(6)	N2–Mg1–N8	87.63(8)	86.61(8)	86.7
O2–Mg2–N10	104.59(7)	O1–Mg1–N2	104.28(8)	103.64(9)	103.7
O2–Mg2–N12	102.84(7)	O1–Mg1–N4	100.82(8)	100.07(8)	104.4
O2–Mg2–N14	102.35(7)	O1–Mg1–N6	101.48(8)	101.66(9)	104.5
O2–Mg2–N16	103.98(7)	O1–Mg1–N8	105.16(8)	105.19(9)	104.1
Deviation of Mg from the $N_4$ -plane	0.474(2)		0.456(1)	0.445(1)	0.505

**Table 7**  
Hydrogen-bond geometry ( $\text{\AA}$ ,  $^\circ$ ) in **4**.

$D-H\cdots A$	$D-H$	$H\cdots A$	$D\cdots A$	$D-H\cdots A$
O1–H1O1 $\cdots$ N1 <sup>i</sup>	0.82(1)	2.18(1)	2.995(2)	171(3)
O1–H2O1 $\cdots$ N17	0.82(1)	1.97(1)	2.784(3)	173(3)

Symmetry code: (i)  $-x, -y + 1, -z + 1$ .

the  $[\text{MgPc}(\text{DMSO})]_2$  dimers with ordered and disordered axial DMSO ligand, respectively. These dimers are further organised in the stacking structure (Fig. 8c). The  $[\text{MgPc}(\text{DMSO})]_2$  dimers with ordered axial DMSO ligands related by translation are oriented in the back-to-back fashion with an interplanar  $N_4-N_4$  distance of  $3.442(2)$   $\text{\AA}$  between the saucer-shaped  $\text{Pc}^{2-}$  macrocycles forming

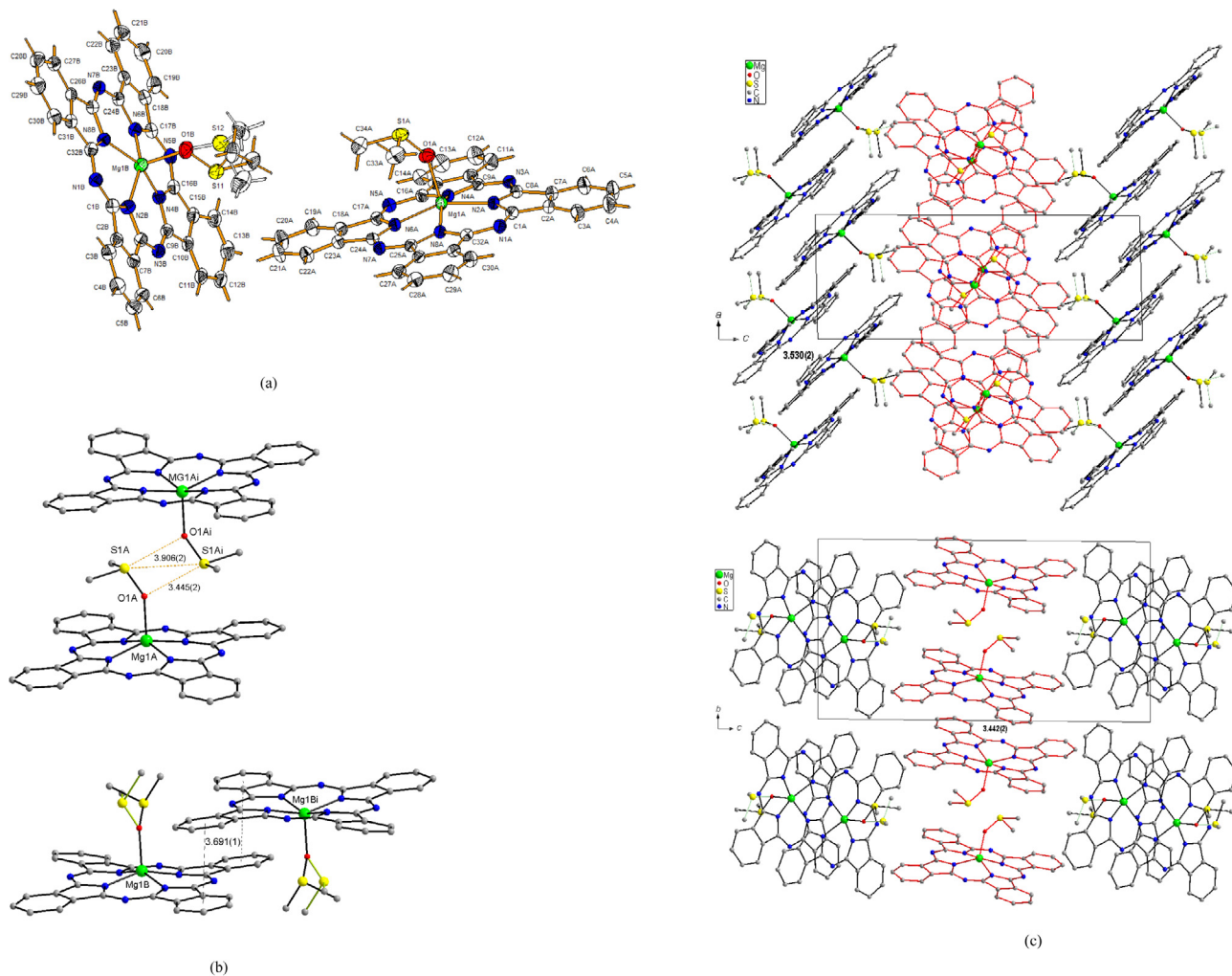


**Fig. 8.** View of the molecular structure of **5** along with the labelling scheme, thermal ellipsoids are shown at the 50% probability level, H atoms with arbitrary radii (a) and the face to face dimers of  $[(\text{MgPc}(\text{DMSO}))_2]$  with ordered and disordered DMSO (b) and the crystal packing showing the  $N_4-N_4$  distances between the back-to-back units in **5**, the  $[(\text{MgPc}(\text{DMSO}))_2]$  units with disordered and ordered DMSO are shown in black and red, respectively (c).

stacks along *b*-axis, whereas the other dimers with disordered axial DMSO ligands related by translation are oriented in the back-to-back fashion, with an interplanar N<sub>4</sub>–N<sub>4</sub> distance of 3.530(2) Å, forming stacks along *a*-axis (Fig. 8c). Thus the alternative arrangement of the [MgPc(DMSO)]<sub>2</sub> dimers in the stacks is determined by the  $\pi$ – $\pi$  interaction within the stacks, whereas the van der Waals forces are responsible for the interstacking interactions. These  $\pi$ – $\pi$  interaction within the stacks is less effective due to the saucer-shaped form of Pc<sup>2-</sup> macrocycles, so the solubility is ~5 times greater comparing to that of the parent MgPc pigment.

### 3.3.6. Mg(acac)<sub>2</sub>(H<sub>2</sub>O)<sub>2</sub> – (6) and C<sub>10</sub>H<sub>12</sub>O<sub>2</sub> – (7)

Compound **6** crystallises in the centrosymmetric space group P 2<sub>1</sub>/c of the monoclinic system with two molecules per unit cell. Asymmetric unit of **6** consists of half Mg(acac)<sub>2</sub>(H<sub>2</sub>O)<sub>2</sub> molecule since the Mg lies in the inversion. The Mg<sup>2+</sup> cation is chelated by two acac<sup>-</sup> anions forming distorted square planar coordination and by two water molecules in the axial positions, above and below the square plane of MgO<sub>4</sub> forming elongated square bipyramid (Fig. 9a). The four equatorial Mg–O bonds linking the Mg<sup>2+</sup> with chelate acac<sup>-</sup> anions are shorter by ~0.1 Å than the axial bonds linking the Mg<sup>2+</sup> with water molecules (Table 8). Due to the chelating effect the O–Mg–O angle with both O atoms belonging to the same acac<sup>-</sup> anion is slightly smaller than the other O–Mg–O angle with oxygen atoms coming from different acac<sup>-</sup> ligands. The carbon chain together with the oxygen atoms of acac<sup>-</sup> are almost planar. Quite similar bipyramidal environment of Mg atom of Mg(acac)<sub>2</sub>(H<sub>2</sub>O)<sub>2</sub> complex is preferred in solution and in the gas-phase as is evidenced by the DFT molecular orbital calculations, however the calculated axial Mg–O is slightly longer than in the crystal (Table 8). Full geometrical parameters of the optimised conformation of the MgPc(acac)<sub>2</sub>(H<sub>2</sub>O)<sub>2</sub> molecule are listed in Supplementary (Table S4). Arrangement of MgPc(acac)<sub>2</sub>(H<sub>2</sub>O)<sub>2</sub> molecules in the crystal is determined by the O–H...O hydrogen bonds (Table 9) formed between the water molecules of one

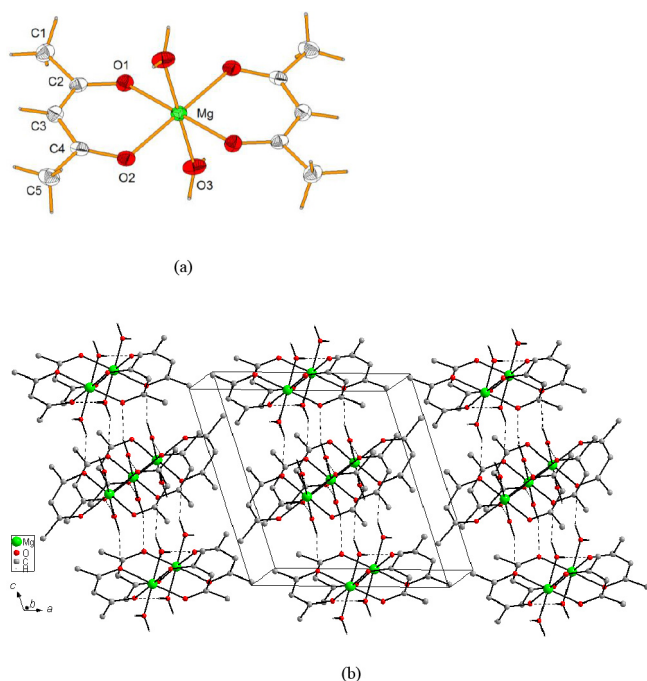


**Fig. 9.** View of the molecular structure of **6** along with the labelling scheme, thermal ellipsoids are shown at the 50% probability level, H atoms with arbitrary radii (a) and the crystal packing of **6** showing the O–H...O hydrogen bonded layers parallel to (001) plane (b).

**Table 8**  
Selected geometrical parameters (Å, °) for Mg(acac)<sub>2</sub>(H<sub>2</sub>O)<sub>2</sub> – (6).

		X-ray	DFT
Mg–O1	x2	2.0419(7)	2.046
Mg–O2	x2	2.0299(7)	2.046
Mg–O3	x2	2.1432(8)	2.194
O2–Mg–O1		88.88(3)	86.9
O1–Mg–O3		88.95(3)	86.0
O2–Mg–O3		91.76(3)	86.1
O1–Mg–O2 <sup>i</sup>		91.12(3)	93.1
O1–Mg–O3 <sup>i</sup>		91.05(3)	94.0
O2–Mg–O3 <sup>i</sup>		88.24(3)	93.9
C1–C2–C3–C4		174.65(9)	178.9
C2–C3–C4–C5		179.64(9)	–178.9
O1–C2–C3–C4		–4.95(15)	–0.6
C2–C3–C4–O2		–0.26(15)	0.6

Symmetry code: (i)  $-x + 1, -y + 1, -z + 1$ .

**Table 9**  
Hydrogen-bond geometry (Å, °) in **6**.

D–H–A	D–H	H–A	D–A	D–H–A
O3–H31–O1 <sup>ii</sup>	0.84(2)	2.09(2)	2.928(1)	174(1)
O3–H32–O2 <sup>iii</sup>	0.87(2)	2.12(2)	2.930(1)	155(1)

Symmetry codes: (ii)  $-x + 1, -y, -z + 1$ ; (iii)  $-x + 1, y - 1/2, -z + 3/2$ .

MgPc(acac)<sub>2</sub>(H<sub>2</sub>O)<sub>2</sub> molecule with the O atoms of acac<sup>-</sup> of the neighbours MgPc(acac)<sub>2</sub>(H<sub>2</sub>O)<sub>2</sub> molecules, forming layers parallel to the (100) plane (Fig. 9b). Between the layers there are no directional interactions, as hydrogen bonds, and they are arranged each other via van der Waals forces. The van der Waals forces are less effective and the (100) crystallographic plane is a cleavage plane of the crystals.

Compound **7** crystallises in the centrosymmetric space group of the triclinic system with four molecules per unit cell. Asymmetric unit of **7** consists of two independent C<sub>10</sub>H<sub>12</sub>O<sub>2</sub> molecules (Fig. 10). The conformation of both independent molecules are very similar (Table 10). Both 2-acetyl-3,4-dimethylphenol molecules in the crystal are planar (without the H atoms of CH<sub>3</sub> groups), and in both the intramolecular O–H...O hydrogen bond formed between the hydroxyl and carbonyl groups stabilise the planar conformation. Quite similar conformation of 2-acetyl-3,4-dimethylphenol molecule is observed in the gas-phase as is evidenced by the DFT molecular orbital calculations (Table 10). Full geometrical parameters of the optimised conformation of 2-acetyl-3,4-dimethylphenol molecule are listed in Supplementary (Table S5). Arrangement of 2-acetyl-3,4-dimethylphenol molecule with intramolecular O–H...O is mainly determined by the van der Waals forces, since there are no directional interactions between the molecules (Fig. S6).

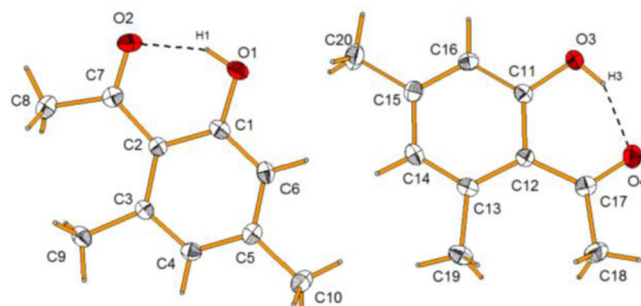


**Fig. 10.** View of the molecular structure of **7** along with the labelling scheme, thermal ellipsoids are shown at the 50% probability level, H atoms with arbitrary radii. Dashed lines represent the intramolecular O–H...O hydrogen bonds.

**Table 10**  
Selected geometrical parameters and the hydrogen-bond geometry (Å,°) for C<sub>10</sub>H<sub>12</sub>O<sub>2</sub> – (7).

				DFT
O1–C1	1.351(2)	O3–C11	1.355(2)	1.341
O2–C7	1.240(2)	O4–C17	1.246(2)	1.248
O1–C1–C2	122.5(1)	O3–C11–C12	122.5(1)	123.0
O2–C7–C2	119.8(1)	O4–C17–C12	119.8(1)	120.4
O1–C1–C2–C3	–179.5(1)	O3–C11–C12–C13	–179.8(1)	–178.8
C8–C7–C2–C1	178.9(1)	C18–C17–C12–C11	176.6(1)	174.1
<i>D</i> – <i>H</i> ·· <i>A</i>	<i>D</i> – <i>H</i>	<i>H</i> ·· <i>A</i>	<i>D</i> ·· <i>A</i>	<i>D</i> – <i>H</i> ·· <i>A</i>
O1–H1··O2	0.82(1)	1.728(1)	2.486(2)	152(2)
O3–H3··O4	0.83(1)	1.721(1)	2.478(2)	152(2)
				DFT
O1–H1··O2	0.999	1.604	2.505	147.5

### 3.4. UV–Vis spectroscopy of MgPc-derivatives 1–5

To further characterize of the MgPc-derivatives 1–5 the electronic absorption spectra were recorded. The spectra of 1–4 complexes were recorded in 3,4-lutidine solutions (Fig. 11) whereas the spectrum of complex 5 was recorded in 3,4-lutidine and DMSO solutions (Fig. 12). The spectra of all complexes 1–5 show two bands (Q and B) characteristic of the phthalocyaninate(2–) macrocycle [82,83]. The Q band of all 1–3 complexes (Fig. 11) is observed at 672 nm ( $\log \epsilon = 6.33$ ) and the B band at  $\sim 350$  nm in the spectrum

of 3,4-lutidine solution. The *N*-coordinated MgPc-derivative, i.e. MgPc(3,4-lut) present in crystal 1 and in co-crystal 3, in 3,4-lutidine solution under air conditions transforms into aquamagnesium phthalocyanine complex, which is more stable at this conditions (Scheme 2), therefore the spectra of 1 and 3 complexes are quite identical with the spectrum of 2. The Q and B bands in the UV–Vis spectrum of MgPc(DMSO) complex (5) in 3,4-lutidine as well as in DMSO solutions (Fig. 12) are blue shifted by  $\sim 10$  nm comparing to that for the 1–3 (Fig. 11). Thus the Q band in the spectrum of MgPc(DMSO) in both solutions is observed at  $\sim 662$  nm ( $\log \epsilon = 6.29$ ) and the B band at  $\sim 340$  nm. In contrast to the *N*-coordinated MgPc-derivative (MgPc(3,4-lut)) that in 3,4-lutidine transforms into aquamagnesium phthalocyanine complex, the MgPc(DMSO) as O-coordinated MgPc-complex is stable in both 3,4-lutidine and DMSO solutions under ambient conditions. The spectrum of 4 which is co-crystal of MgPc(H<sub>2</sub>O) and MgPc(DMSO) in 3,4-lutidine solution is superposition of both MgPc(H<sub>2</sub>O) and MgPc(DMSO) spectrum. This is clearly visible especially in the region of B band (compare the Figs. 11 and 12).

The Q band corresponds to the excitation between the HOMO to LUMO level and the B band corresponds to the HOMO-1 to LUMO level. In addition, the vibronic splitting of the Q band is observed. The splitting value of  $\sim 60$  nm is due to the vibronic coupling in the excited state and was mentioned in the literature [84–86].

To investigate further optical properties of the 1–5 complexes the time-dependent (TD) DFT calculations have been performed. Optical absorption spectra were calculated for MgPc-derivatives present in the 1–5 crystals, i.e. MgPc(3,4-lut), MgPc(H<sub>2</sub>O) and MgPc(DMSO) complexes, and for the parent MgPc pigment, and the results are summarised in Tables S6–S10 (SI). Partial molecular energy diagram, HOMO and LUMO frontier orbitals and the calculated absorption spectra for the MgPc(H<sub>2</sub>O) and MgPc(DMSO) complexes present in solution of 1–5 compounds are shown in Fig. 13. The calculated  $\Delta E$  between HOMO and LUMO orbitals is 2.046 eV (605 nm) for the MgPc(DMSO) complex and is blue shifted by  $\sim 7$  nm in relation to that of the MgPc(H<sub>2</sub>O) complex ( $\Delta E(\text{HOMO}/\text{LUMO}) = 2.025$  eV, 612 nm). Although, there are large number of works reporting the theoretical DFT and TD-DFT calculations performed on tetrapyrrole systems like as porphyrin, porphyrin, texaphyrin, bacteriochlorine, phthalocyanine, naphthalocyanine and their complexes with various metal cations [87–92], the TD-DFT calculations reporting on magnesium phthalocyanine and its axially ligated derivatives are relatively few. For the pure MgPc using the density functional theory and its time dependent approach (TDDFT) in conjunction with the PBE0 exchange-correlation functional and extended TZVP all-electron basis sets yield the HOMO-LUMO energy gap of 2.100 eV (590 nm) [93]. The energy gap between the HOMO and LUMO orbitals calculated for MgPc and its axially ligated by pyridine (MgPcPy) or imidazole (MgPcIm) by TDDFT with the same basis set (6–31+G(d)) is 2.0222 eV

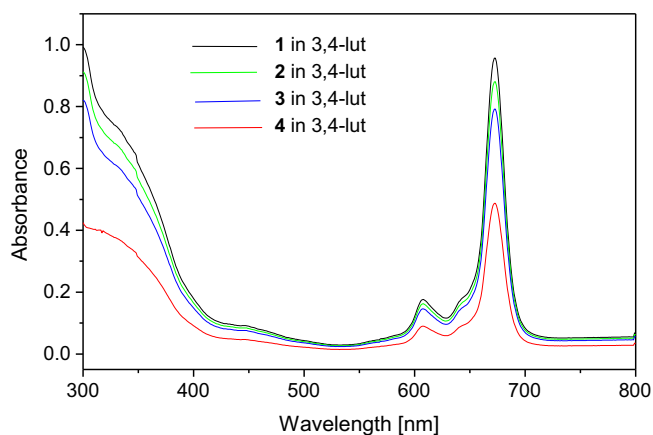


Fig. 11. UV–Vis spectra of 1–4 in 3,4-lutidine solution.

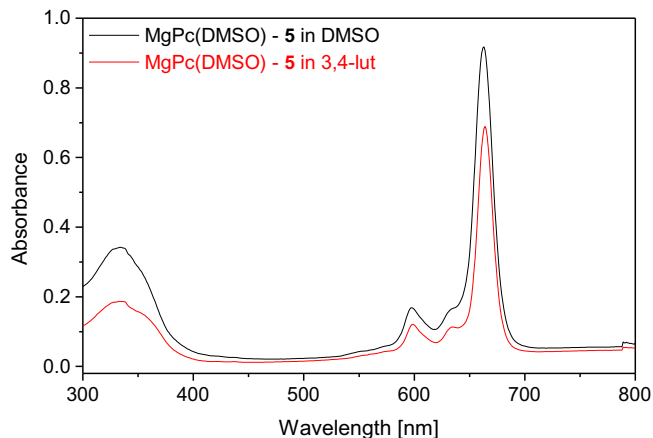
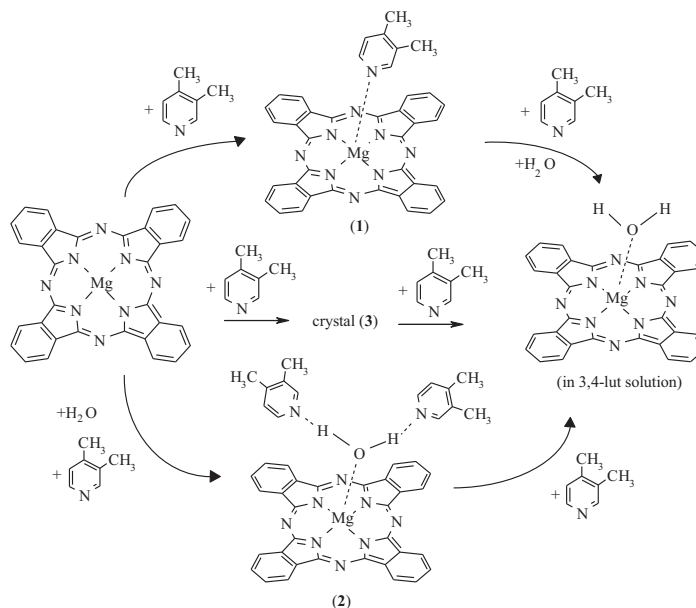


Fig. 12. UV–Vis spectrum of 5 in 3,4-lutidine and DMSO solutions.



Scheme 2. Equilibrium of 1–3 in 3,4-lutidine solution.

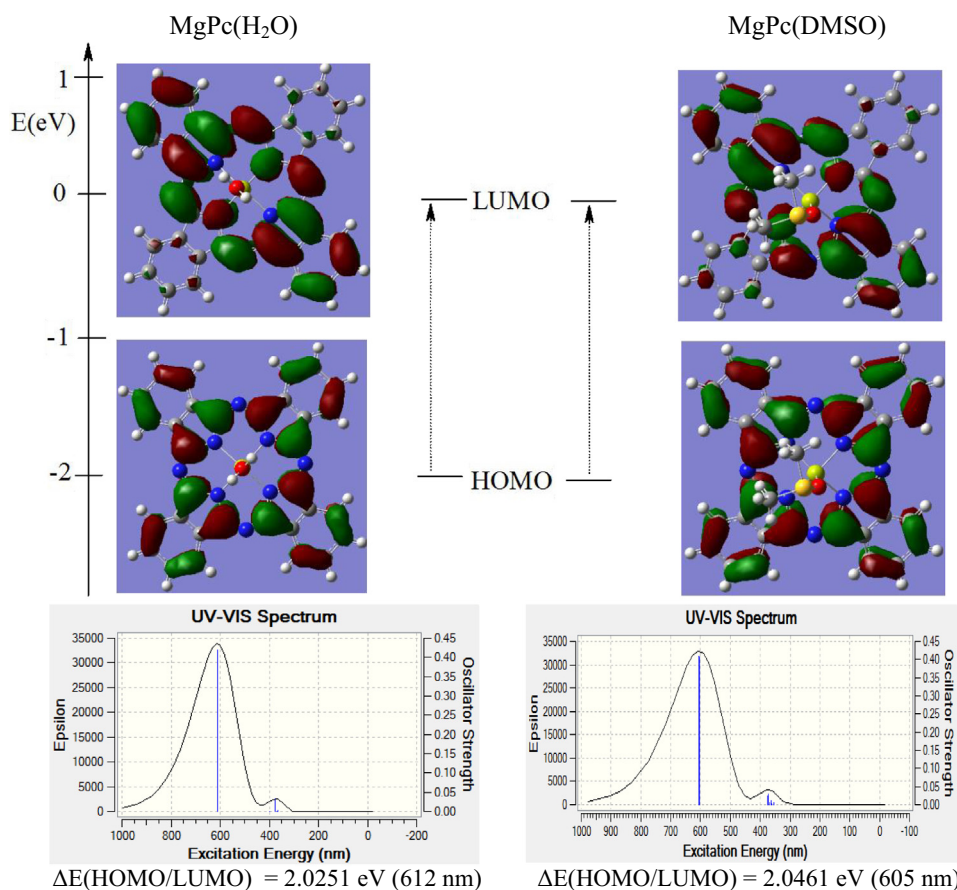


Fig. 13. Partial molecular energy diagram, HOMO and LUMO frontier orbitals and the calculated absorption spectra for the MgPc(H<sub>2</sub>O) and MgPc(DMSO) complexes.

(616 nm), 2.0141 eV (613 nm) and 2.0358 eV (609 nm), respectively [75]. Aromatic macrocycles including metallophthalocyanines are extensively studied as photosensitizers in a non-invasive treatment (photodynamic therapy, PDT). The photosensitizer should have a strong absorption in the therapeutic window

(600–900 nm). Moreover, the energy gap should be greater than or equal to 22.5 kcal/mol [93,94]. In PDT, a photosensitizer in its ground state ( $S_0$ ) first absorbs energy and is excited to its shorter-lived first excited state ( $S_1$ ), then undergoes conversion to the first excited triplet state by intersystem crossing. The triplet

state of the photosensitizer can release its energy to the surrounding biological tissue exciting the oxygen from its triplet to the highly active singlet state, that will eventually kill targeted cells. The investigated here axially ligated magnesium phthalocyanine complexes have a sufficient energy gap to excite ground state of oxygen, and in addition the magnesium phthalocyanine derivatives are non-toxic and can be tested as potential photosensitizers. The calculated HOMO-LUMO transition for the MgPc(H<sub>2</sub>O) and MgPc(DMSO) complexes is shifted by ~50 nm in relation to that of experimental value, however the difference between the  $\lambda_{\text{max}}$  of the Q band of these complexes is comparable with the experimental results. Quite similar discrepancy between experimental and theoretical Q values for the magnesium phthalocyanine axially ligated by pyridine (MgPcPy) or imidazole (MgPcIm) was found [75]. The electronic absorption spectrum for the parent MgPc pigment was also calculated for a comparison (Table S6 and Fig. S7). These results point that axial ligation of MgPc by O- and N-donor ligands do not change significantly the descriptors of the Q band, including the transition energy, the oscillator strength and the main configuration when compared with that of the parent MgPc pigment (Table S6 in SI).

#### 4. Conclusion

This work clearly demonstrates, that even MgPc as the aromatic compound can react under solvothermal conditions leading to the MgPc derivatives or to other compounds that results as a consequence of the demetallation. Solvothermal reaction of MgPc in dry 3,4-lutidine, in 3,4-lutidine/DMSO, in DMSO and in 3,4-lutidine/acetylacetone systems leads to formation new compounds in the crystalline form. In dry 3,4-lutidine the MgPc forms axially ligated 4 + 1 MgPc-derivative (MgPc(3,4-lut) – **1**), which is in contrast to solvothermal reaction of MgPc in 3,5-lutidine that leads to the biaxial ligation and formation of 4 + 2 coordinated MgPc-derivative. Depending on the quantity of the DMSO in the 3,4-lutidine/DMSO system three 4 + 1 coordinated MgPc-derivatives: MgPc(H<sub>2</sub>O)·2(3,4-lut) – (**2**), [MgPc(3,4-lut)] [MgPc(H<sub>2</sub>O)·2(3,4-lut)]·½(3,4-lut) – (**3**) and [MgPc(H<sub>2</sub>O)·(3,4-lut)] [MgPc(DMSO)]·½(DMSO) – (**4**) are formed. The presence of water in the formed **2–4** crystals results from a high affinity of MgPc to water. Solvothermal reaction of MgPc in DMSO leads to formation of monoaxially ligated by DMSO MgPc-derivative (**5**). The coordination environment of the Mg center of MgPc molecule exhibits 4 + 1 coordination independent on the N- or O- ligands. As a ligation result, for the N-ligated MgPc derivatives, the four equatorial Mg-N<sub>iso</sub> bonds elongate but they are still shorter than the axial Mg-N bond. However, for the O-ligated MgPc complexes the opposite relation between the equatorial Mg-N<sub>iso</sub> and the axial Mg-O bonds is observed. Solvothermal reaction of MgPc in 3,4-lutidine/acetylacetone system leads to demetallation of MgPc and formation of the Mg(acac)<sub>2</sub>(H<sub>2</sub>O)<sub>2</sub> complex (**6**) in the crystalline form that in the mother liquor transforms into organic compound C<sub>10</sub>H<sub>12</sub>O<sub>2</sub> (**7**). Partial MO energy diagram and the TD-DFT calculated electronic spectra of the obtained MgPc-derivatives were compared with the experimental electronic absorption spectra in solutions. These results point that the ligation of MgPc by O- and N-donating ligands do not change significantly the energy gap of the HOMO-LUMO level of the 4 + 1 coordinated MgPc derivatives with the O- or N- axial ligands.

#### Acknowledgement

Calculations have been carried out using resources provided by Wrocław Centre for Networking and Supercomputing (<http://www.wcss.wroc.pl>).

#### Appendix A. Supplementary data

Additional material comprising the thermogravimetric analysis of **1–5** and the DFT optimized parameters for MgPc(3,4-lut), MgPc(H<sub>2</sub>O), MgPc(DMSO), Mg(acac)<sub>2</sub>(H<sub>2</sub>O)<sub>2</sub> and the C<sub>10</sub>H<sub>12</sub>O<sub>2</sub>, and the TD-DFT output for MgPc and the MgPc-derivatives. Full details of the X-ray data collection and final refinement parameters including anisotropic thermal parameters and full list of the bond lengths and angles have been deposited with the Cambridge Crystallographic Data Center in the CIF format as supplementary publications no. CCDC 1573169, 1573170, 1573171, 1573172, 1573173, 1573174, 1573175 for **1–7** compounds, respectively. Copies of the data can be obtained free of charge on the application to CCDC, 12 Union Road, Cambridge, CB21EZ, UK, (fax: (+44) 1223-336-033; email: deposit@ccdc.cam.ac.uk). Supplementary data associated with this article can be found, in the online version, at <http://doi.org/10.1016/j.ica.2018.03.018>.

#### References

- [1] R.P. Linstead, *J. Chem. Soc.* (1934) 1016–1017.
- [2] C.C. Leznoff, A.B.P. Lever, *Phthalocyanines: Properties and Applications*, VCH Publishers, New York, 1996.
- [3] P. Gregory, *J. Porphyrins Phthalocyanines* 4 (2000) 432–437.
- [4] N.B. MacKeown, *Phthalocyanine Materials, Structure and Functions*, Cambridge University Press, Cambridge, 1998.
- [5] G. Guillard, J. Simon, J.P. Germain, *Coord. Chem. Rev.* 178–180 (1998) 1433–1484.
- [6] G. Torre, P. Vázquez, F. Agulló-López, T. Torres, *Chem. Rev.* 104 (2004) 3723–3750.
- [7] M. Calvete, G.Y. Yang, M. Hanack, *Synth. Met.* 141 (2004) 231–243.
- [8] S. Baranton, C. Coutanceau, C. Roux, F. Hahn, J.M. Léger, *J. Electroanal. Chem.* 577 (2005) 223–234.
- [9] M.V. Martínez-Díaz, M. Ince, T. Torres, *Monatsh. Chem.* 142 (2011) 699–707.
- [10] D. Wöhrle, G. Schnurpfeil, S.G. Makarov, A. Kazarin, O.N. Suvorova, *Macrocyclics* 5 (2012) 191–202.
- [11] R. Bonnett, *Chem. Soc. Rev.* 24 (1995) 19–33.
- [12] R. Bonnett, *Chemical Aspects of Photodynamic Therapy*, Gordon and Breach Science Publishers, Amsterdam, 2000.
- [13] E.A. Lukyanets, *J. Porphyrins Phthalocyanines* 3 (1999) 424–432.
- [14] A.E. O'Connor, W.M. Gallagher, A.T. Byrne, *Photochem. Photobiol.* 85 (2009) 1053–1074.
- [15] P. Skupin-Mrugalska, J. Piskorz, T. Goslinski, J. Mielcarek, K. Konopka, N. Düzgünes, *Drug Discov. Today* 18 (2013) 776–784.
- [16] S. Yano, S. Hirohara, M. Obata, Y. Hagiya, S. Ogura, A. Ikeda, H. Kataoka, M. Tanaka, T. Joh, *J. Photochem. Photobiol. C* 12 (2011) 46–67.
- [17] S.S. Lucky, K.C. Soo, Y. Zhang, *Chem. Rev.* 115 (2015) 1990–2042.
- [18] L.P. Vernon, G.R. Seely (Eds.), *The Chlorophyll*, Academic Press, New York, 1966.
- [19] J. Janczak, R. Kubiak, *Polyhedron* 20 (2001) 2901–2909.
- [20] R. Kubiak, J. Janczak, K. Ejsmont, *Chem. Phys. Lett.* 245 (1995) 249–252.
- [21] J. Janczak, R. Kubiak, *Polyhedron* 56 (2013) 200–210.
- [22] J. Janczak, Y.M. Idemori, *Polyhedron* 22 (2003) 1167–1181.
- [23] M. Hanack, A. Gül, A. Hirsch, B.K. Mandal, L.R. Subramanian, W. Witke, *Mol. Cryst. Liq. Cryst.* 187 (1990) 365–382.
- [24] M.P. Donzello, Z. Ou, D. Dini, M. Meneghetti, C. Ercolani, K.M. Kadish, *Inorg. Chem.* 43 (2004) 8637–8648.
- [25] X. Deng, W.W. Porter, T.P. Vaid, *Polyhedron* 24 (2005) 3004–3011.
- [26] F. Yuksel, D. Atilla, V. Ahsen, *Polyhedron* 26 (2007) 4551–4556.
- [27] J. Mack, N. Kobayashi, *Chem. Rev.* 111 (2011) 281–321.
- [28] E. Tuğba, D. Çakir, Z. Biyiklioğlu, H. Kantekin, *Dyes Pigments* 98 (2013) 255–262.
- [29] H. Dumrul, F. Yuksel, *Polyhedron* 63 (2013) 83–90.
- [30] J. Janczak, R. Kubiak, *Polyhedron* 21 (2002) 265–274.
- [31] R. Kubiak, J. Janczak, M. Śledź, E. Bukowska, *Polyhedron* 26 (2007) 4179–4186.
- [32] J. Janczak, R. Kubiak, *CrystEngComm* 12 (2010) 3599–3606.
- [33] B. Przybył, J. Janczak, *Dyes Pigments* 130 (2016) 54–62.
- [34] B. Assmann, G. Ostendorf, G. Lehmann, H. Homborg, *Z. Anorg. Allg. Chem.* 622 (1996) 1085–1090.
- [35] H. Hückstädt, C. Jaouen, M. Göldner, U. Cornelissen, A. Tutass, H. Homborg, *Z. Anorg. Allg. Chem.* 626 (2000) 671–678.
- [36] E.A. Lukyanets, V.N. Nemykin, *J. Porphyrins Phthalocyanines* 14 (2010) 1–40.
- [37] J. Mack, N. Kobayashi, *Chem. Rev.* 111 (2011) 281–321.
- [38] H. Lu, N. Kobayashi, *Chem. Rev.* 116 (2016) 6184–6261.
- [39] V.I. Vlaskin, O.P. Dimitriev, Z.I. Kazantseva, A.V. Nabok, *Thin Solid Films* 286 (1996) 40–44.
- [40] H. Isago, C.C. Leznoff, M.F. Pyan, R.A. Metcalfe, R. Davids, A.B.P. Lever, *Bull. Chem. Soc. Jpn.* 71 (1998) 1039–1047.
- [41] K. Adachi, H. Watarai, *Bull. Chem. Soc. Jpn.* 77 (2004) 2011–2020.

- [42] J. Janczak, R. Kubiak, M. Śledź, H. Borrmann, Y. Grin, *Polyhedron* 22 (2003) 2689–2697.
- [43] J. Janczak, *Polyhedron* 30 (2011) 2933–2940.
- [44] J. Janczak, R. Kubiak, J. Lisowski, *Polyhedron* 30 (2011) 253–258.
- [45] J. Janczak, R. Kubiak, J. Lisowski, *J. Porphyrins Phthalocyanines* 17 (2013) 742–749.
- [46] B. Przybył, J. Janczak, *Dyes Pigments* 100 (2014) 247–254.
- [47] J. Janczak, *Polyhedron* 70 (2014) 164–171.
- [48] J. Janczak, R. Kubiak, *Inorg. Chim. Acta* 376 (2011) 28–35.
- [49] J. Janczak, R. Kubiak, *Eur. J. Inorg. Chem.* (2014) 1105–1115.
- [50] J. Janczak, R. Kubiak, *Polyhedron* 81 (2014) 695–704.
- [51] J. Janczak, *Polyhedron* 38 (2012) 75–87.
- [52] V. Kinzhybalov, R. Kubiak, J. Janczak, *Polyhedron* 115 (2016) 142–154.
- [53] CrysAlis CCD and CrysAlis Red 1.171.38.41, Rigaku Oxford Diffraction, 2015.
- [54] G.M. Sheldrick, SHELXS97, Programs for Crystal Structures Solution and Refinement, University of Göttingen, Göttingen, Germany, 1997.
- [55] G.M. Sheldrick, *Acta Cryst. C* 71 (2015) 3–8.
- [56] K. Brandenburg, H. Putz, DIAMOND Version 3.0, Crystal Impact GbR, Bonn, Germany, 2006.
- [57] M. J. Frisch, G. W. Trucks, H. B. Schlegel, G. E. Scuseria, M. A. Robb, J. R. Cheeseman, G. Scalmani, V. Barone, B. Mennucci, G. A. Petersson, H. Nakatsuji, M. Caricato, X. Li, H. P. Hratchian, A. F. Izmaylov, J. Bloino, G. Zheng, J. L. Sonnenberg, M. Hada, M. Ehara, K. Toyota, R. Fukuda, J. Hasegawa, M. Ishida, T. Nakajima, Y. Honda, O. Kitao, H. Nakai, T. Vreven, J. A. Montgomery, Jr., J. E. Peralta, F. Ogliaro, M. Bearpark, J. J. Heyd, E. Brothers, K. N. Kudin, V. N. Staroverov, T. Keith, R. Kobayashi, J. Normand, K. Raghavachari, A. Rendell, J. C. Burant, S. S. Iyengar, J. Tomasi, M. Cossi, N. Rega, J. M. Millam, M. Klene, J. E. Knox, J. B. Cross, V. Bakken, C. Adamo, J. Jaramillo, R. Gomperts, R. E. Stratmann, O. Yazyev, A. J. Austin, R. Cammi, C. Pomelli, J. W. Ochterski, R. L. Martin, K. Morokuma, V. G. Zakrzewski, G. A. Voth, P. Salvador, J. J. Dannenberg, S. Dapprich, A. D. Daniels, O. Farkas, J. B. Foresman, J. V. Ortiz, J. Cioslowski, and D. J. Fox, Gaussian, Inc., Wallingford CT, 2013. Gaussian09, Revision D.01, Programme, Gaussian, Inc., Wallingford, CT, 2013.
- [58] A.D. Becke, *J. Chem. Phys.* 104 (1996) 1040–1046.
- [59] C. Lee, W. Yang, R.G. Parr, *Phys. Rev. B* 37 (1988) 785–789.
- [60] B.G. Parr, W. Yang, *Density-Functional Theory of Atoms and Molecules*, Oxford University Press, New York, 1989.
- [61] R. Bauernschmitt, R. Ahlrichs, *Chem. Phys. Lett.* 256 (1996) 454–464.
- [62] A. Dreuw, M. Head-Gordon, *Chem. Rev.* 105 (2005) 4009–4037.
- [63] P. Politzer, P.R. Laurence, K. Jayasuriya, *Environ. Health Perspect.* 61 (1985) 191–202.
- [64] P. Politzer, P. Lane, *Struct. Chem.* 1 (1990) 159–164.
- [65] P. Sjöberg, P. Politzer, *J. Phys. Chem.* 94 (1990) 3959–3961.
- [66] C.A. Hunter, *Angew. Chem. Int. Ed.* 43 (2004) 5310–5324.
- [67] P. Politzer, J. S. Murray, In *Comput. Med. Chem. Drug Discovery*, P. Bultinck, P. H. De Winter, W. Langenaeker, J. P. Tollenaere, (Eds.) New York: Marcel Dekker Inc; 2004. pp. 213–234.
- [68] M. Zerner, M. Gouterman, H. Kobayashi, *Theoret. Chim. Acta* 6 (1966) 363–400.
- [69] R.G. Pearson, *J. Am. Chem. Soc.* 85 (1963) 3533–3539.
- [70] R.G. Pearson, J. Songstad, *J. Am. Chem. Soc.* 89 (1967) 1827–1836.
- [71] R.G. Pearson, *J. Chem. Educ.* 76 (1999) 267–275.
- [72] W. Caminati, J.U. Grabow, *J. Am. Chem. Soc.* 128 (2006) 854–857. and refs cited therein.
- [73] J. Stary, J.O. Liljenzin, *Pure & Appl. Chem.* 54 (1982) 2557–2592.
- [74] J. Janczak, R. Kubiak, E. Bukowska, *J. Mol. Struct.* 937 (2009) 25–33.
- [75] Y. Yang, *J. Phys. Chem. A* 115 (2011) 9043–9054.
- [76] J. Mizuguchi, *Z. Kristallogr.* NCS 217 (2002) 251–252.
- [77] V. Kinzhybalov, J. Janczak, *J. Mol. Struct.* 996 (2011) 64–68.
- [78] H.C. Chow, R. Serlin, C.E. Strouse, *J. Am. Chem. Soc.* 97 (1975) 7230–7237.
- [79] C. Kratky, J.D. Dunitz, *Acta Cryst. B* 33 (1977) 545–547.
- [80] V. Gutmann, *Electrochim. Acta* 21 (1976) 661–670.
- [81] K.M. Kadish, D.J. Leggett, D. Chang, *Inorg. Chem.* 21 (1982) 3618–3622.
- [82] L. Edwards, M.J. Gouterman, *J. Mol. Spectrosc.* 33 (1970) 292–310.
- [83] M. J. Stillman, T. Nykong, in C. C. Leznoff, A.B.P. Lever, (Eds.), *Phthalocyanines: Properties and Applications*, Vol. 1, VCH Publishers Inc., New York, 1989, p.138.
- [84] T. Nykong, Z. Gasyina, M.J. Stillman, *Inorg. Chem.* 26 (1987) 1087–1095.
- [85] T. Reinot, J.M. Hayes, G.J. Smal, C. Zerner, *Chem. Phys. Lett.* 299 (1999) 410–416.
- [86] K. Liu, Y. Wang, J. Yao, Y. Luo, *Chem. Phys. Lett.* 438 (2007) 36–40.
- [87] J. Mack, M.J. Stillman, *J. Am. Chem. Soc.* 116 (1994) 1294–1304.
- [88] J. Mack, M.J. Stillman, *Inorg. Chem.* 36 (1997) 413–425.
- [89] G. Ricciardi, A. Rosa, E.J. Baerends, *J. Phys. Chem. A* 105 (2001) 5242–5254.
- [90] M. Pia Donzello, C. Eroclani, K.M. Kadish, G. Ricciardi, A. Rosa, P.A. Stuzhin, *Inorg. Chem.* 46 (2007) 4145–5157.
- [91] X. Liang, J. Mack, L.M. Zheng, Z. Shen, N. Kobayashi, *Inorg. Chem.* 53 (2014) 2797–2802.
- [92] J. Mack, *Chem. Rev.* 117 (2017) 3444–3478.
- [93] I. Lanzao, N. Russo, E. Sicilia, *J. Phys. Chem. B* 112 (2008) 4123–4130.
- [94] A.D. Quartarolo, S.G. Chiodo, N. Russo, *J. Chem. Theory Comput.* 6 (2010) 3176–3189.